# Finite-Cardinality Single-RF Differential Space-Time Modulation for Improving the Diversity-Throughput Tradeoff

Chao Xu, *Member, IEEE,* Peichang Zhang, *Member, IEEE,* Rakshith Rajashekar, *Senior Member, IEEE,* Naoki Ishikawa, *Student Member, IEEE,* Shinya Sugiura, *Senior Member, IEEE,* Li Wang, *Member, IEEE,* and Lajos Hanzo* *Fellow, IEEE*

***Abstract*—The matrix-based differential encoding invoked by Differential Space-Time Modulation (DSTM) typically results in an infinite-cardinality of arbitrary signals, despite the fact that the Transmit Antennas (TAs) can only radiate a limited number of patterns. As a remedy, the recently developed Differential Spatial Modulation (DSM) is capable of avoiding this problem by conceiving a beneficial sparse signal matrix design, which also facilitates low-complexity single-RF signal transmission. Inspired by this development, the Differential Space-Time Block Code using Index Shift Keying (DSTBC-ISK) further introduces a beneficial diverstiy gain without compromising the DSM's appealingly low transceiver complexity. However, the DSTBC-ISK's performance advantage tends to diminish as the throughput increases, especially when an increased number of Receive Antennas (RAs) is used. By contrast, the classic Differential Group Code (DGC) that actively maximizes its diversity gain for different Multiple-Input Multiple-Output (MIMO) system setups is capable of achieving a superior performance, but its detection complexity grows exponentially with the throughtput. Against this background, we propose the Differential Space-Time Shift Keying using Diagonal Algebraic Space-Time (DSTSK-DAST) scheme, which is the first DSTM that is capable of achieving the DGC's superior diversity gain at high throughputs without compromising the DSM's low transceiver complexity. As a further advance, we also conceive a new Differential Space-Time Shift Keying using Threaded Algebraic Space-Time (DSTSK-TAST) arrangement, which is capable of achieving an even further improved diversity gain at a substantially reduced signal detection complexity compared to the best DGCs. Furthermore, in order to strike a practical tradeoff, we develop a generic multi-element and multi-level-ring Amplitude Phase Shift Keying (APSK) design, and we also arrange for multiple reduced-size DSTM sub-blocks to be transmitted in a permuted manner, which exhibits an improved diversity-throughput tradeoff.**

***Index Terms*—Differential space-time modulation, differential spatial modulation, diagonal algebraic space-time, threaded algebraic space-time, space-time shift keying, group code, single-RF, finite-cardinality, single-stream ML detection, diversity gain, throughput-diversity tradeoff.**

C. Xu, R. Rajashekar and L. Hanzo are with the School of Electronics and Computer Science, University of Southampton, Southampton SO17 1BJ, UK (e-mail: {cx1g08,rmr1u14,lh}@soton.ac.uk).

P. Zhang is with College of Information Engineering, Shenzhen University, Shenzhen 518060, China (e-mail: pzhang@szu.edu.cn).

N. Ishikawa is with the Graduate School of Information Sciences, Hiroshima City University, Ohzuka-higashi 731-3194, Japan (e-mail: naoki@ishikawa.cc).

S. Sugiura is with the Institute of Industrial Science, University of Tokyo, Meguro-ku, Tokyo 153-8505, Japan (e-mail: sugiura@ieee.org).

L. Wang is with Huawei Technology Sweden R&D Competence Center (e-mail: leo.li.wang@huawei.com).

This work was supported in part by the EPSRC projects EP/Noo4558/1 and EP/PO34284/1, the European Research Council's Advanced Fellow Grant under the QuantCom project and the Royal Society's Wolfson Research Merit Award and the GRCF. The work of N. Ishikawa was supported in part by the Japan Society for the Promotion of Science KAKENHI under Grant 17H07036. The work of S. Sugiura was supported in part by the Japan Society for the Promotion of Science KAKENHI under Grants 26709028 and 16KK0120.

## I. INTRODUCTION

Differential Space-Time Modulation (DSTM) constitutes a low-complexity design alternative to coherent Multiple-Input Multiple-Output (MIMO) schemes, where the excessive pilot overhead and the high-complexity channel estimation can be eliminated. Based on the classic Space-Time Block Codes (STBCs) [1]–[3], Differential STBCs (DSTBCs) were conceived in [4]–[6]. Moreover, based on the family of Linear Dispersion Codes (LDCs) [7]–[11] that are capable of achieving both the V-BLAST's high throughput and the STBC's full diversity, Differential LDCs (DLDCs) were conceived in [12], [13], where the Cayley transform was invoked in order to employ unitary signal matrices. The recently developed Differential Space-Time Shift Keying (DSTSK) [14]–[16] avoids the non-linear Cayley transform, where only a single unitary dispersion matrix is activated. As a benefit of the unitary and linear design, both DSTBC and DSTSK are capable of decoupling the received signals, where the single-stream ML detection complexity does not grow with the constellation size [6], [17], [18].

In contrast to both the DPSK [19], [20] and star QAM schemes [21]–[25] routinely used in Single-Input Single-Output (SISO) channels, the matrix multiplication invoked by the DSTM's differential encoding results in arbitrary infinite-cardinality of transmit signals for all the aforementioned DSTM schemes. However, in reality, the Transmit Antennas (TAs) can only radiate a limited number of signal transmission patterns [26]–[28]. As a remedy, inspired by the recently proposed Spatial Modulation (SM) [17], [18], [29], [30], the Differential SM (DSM) concept was investigated in [31]–[34], while their applications in the future wireless networks were also received in [35], [36]. More explicitly, the finite-cardinality of the classic PSK/QAM constellations was retained thanks to the DSM's beneficial sparse matrix design, which also facilitates low-complexity single-RF signal transmission. However, the DSM does not perform well, when the number of Receive Antennas (RAs) $N$ is low. In order to introduce a beneficial transmit diversity gain, Field Extension based DSM (FE-DSM) was conceived in [37], and then it was refined in [38] in order to generate a finite-cardinality signal set, which became a special case of the DGC $G_{m,r}$ of [39] associated with $r = 1$. Moreover, the recently proposed DSTBC using Index Shift Keying (DSTBC-ISK) [40] transformed the DSTBC signals [4]–[6] to finite-cardinality sets by activating only a single modulated symbol in the STBC's signal structure. Although FE-DSM and DSTBC-ISK significantly outperform DSM at low throughputs, their diversity gains tend to diminish as the throughput increases, especially when a higher number of RAs is used.

As a remedy, the classic Differential Group Code (DGC) [39], [41]–[43] that forms a finite group may be invoked, where the diversity gain is consciously maximized by rotating the PSK signal elements for different Multiple-Input Multiple-Output (MIMO) system setups. However, owing to the associated non-linear phase rotations imposed on the data-carrying PSK signal, the DGC's ML detection complexity grows exponentially with the throughtput. In summary, the family of DSTM schemes is characterized in terms of its transceiver complexity versus its performance in Table I. We note that for a generic DSTM, the notations $M$, $N$, $T$ and $Q$ represent the numbers of TAs, RAs, transmission time slots and dispersion matrices, respectively. The cardinality of the DSTM's data-carrying matrix set is denoted by $I$, hence the throughput is $R = \frac{\log_2 I}{T}$. *Against this background, our objective is to mitigate the problem of the diminishing diversity gain of FE-DSM and DSTBC-ISK, by invoking the DGC's diversity gain maximization, without compromising the DSM's low transceiver complexity.* More explicitly, the novel contributions of this paper are:

1) We propose a new DSTSK using Diagonal Algebraic Space-Time (DSTSK-DAST) coding. First of all, we portray the DAST of [7] as a LDC scheme using $Q$ dispersion matrices. Then the proposed DSTSK-DAST transforms the LDC's 'matrix-multiplexing' form into the STSK's 'matrix-activation' form, where $\log_2 Q$ bits are assigned to activate a single one out of $Q$ dispersion matrices. In order to retain a **finite-cardinality** signal set, we opt for confining the elements in the DSTSK-DAST's dispersion matrices to an equi-spaced $L_{DM}$-PSK constellation. As a result, on one hand, the DSTSK's **single-stream ML detection** is invoked without imposing any performance loss. On the other hand, the DGC's phase rotation method is applied to the $L_{DM}$-PSK elements in the dispersion matrices, so that the DSTSK-DAST's **diversity gain** is actively maximized for different MIMO setups.
2) Furthermore, we propose a new DSTSK using Threaded Algebraic Space-Time (DSTSK-TAST) scheme, which transforms the classic TAST of [10] also into a finite-cardinality single-RF and diversity-gain-maximizing DSTSK scheme. More explicitly, in order to efficiently exploit all the available degrees of freedom, the DSTSK-TAST divides the $(T \times T)$-element space-time signal matrix into $T$ non-overlapping threaded layers, where each threaded layer is a $T$-element vector. Specifically, the DSTSK-DAST's $T$-element diagonal signal vector constitutes one of the threaded layers in the DSTSK-TAST signal structure. As a result, the DSTSK-TAST design may follow the same procedures as the DSTSK-DAST design, but the DSTSK-TAST scheme is capable of conveying $\log_2 T$ extra bits for activating a single one out of $T$ threaded layers for signal transmission.
3) In order to improve the throughput, we extend the Single-Element (SE) Amplitude Phase Shift Keying (APSK) design of [40] to a generic Multi-Element (ME) design. Compared to the existing two/four-level-ring ME APSK solutions of [33], [34], we conceive a single-stream ML detector for the generic family of high-level star QAM signals, where the detection complexity does not grow with the constellation size.
4) Furthermore, in order to strike a practical tradeoff, we arrange for multiple reduced-size DSTM sub-blocks to be transmitted in a permuted manner, which improves Diversity-Rate (DR) tradeoff. This results in an improved throughput at the cost of a reduced diversity gain. Compared to the conventional DR design of [37], [38] using the FE signal matrix, we opt for invoking the layer-swiching matrix of the proposed DSTSK-TAST scheme, so that the resultant bespoke DR design may be applied to the whole family of the diversity-oriented DSTM schemes.

The rest of this paper is organized as follows. The design objectives and preliminaries are presented Sec. II. The new DSTSK-DAST and DSTSK-TAST are proposed in Sec. III and Sec. IV, respectively. The ME APSK design and the DR tradeoff design are detailed in Sec. V. The simulation results are presented in Sec. VI, and our conclusions are offered in Sec. VII

The following notations are used throughout the paper. $\Re(\cdot)$ and $\Im(\cdot)$ represent the real and imaginary parts of complex numbers, respectively. $(\cdot)^*$, $(\cdot)^T$ and $(\cdot)^H$ denote the conjugate of a complex number, the transpose of a matrix and the Hermitian transpose of a complex matrix, respectively. $\otimes$ represents the Kronecker product. tr$(\cdot)$, $rank(\cdot)$ and $\det(\cdot)$ take trace, rank and determinant of a matrix, respectively.

## II. Design Objectives and Preliminaries

In this section, our design objectives are highlighted in the context of the transmitted signal model of Sec. II-A, the received signal model of Sec. II-B as well as the DGC's diversity gain maximization of Sec. II-C. The high-throughput DSM is also briefly reviewed in Sec. II-D.

### A. Transmitted Signal Model

The DSTM's $(T \times M)$-element signal matrix $\mathbf{S}_n$ is obtained by differential encoding:

$$\mathbf{S}_n = \mathbf{X}_{n-1}\mathbf{S}_{n-1}, \tag{1}$$

where we have the constraint of tr$(\mathbf{S}_n^H \mathbf{S}_n) = T$ and $(M \leq T)$, while the $(T \times T)$-element data-signal matrix $\mathbf{X}_{n-1}$ carries source information. The recursion of (1) commences from $\mathbf{S}_1 = \sqrt{\frac{T}{M}}[\mathbf{I}_M, \mathbf{0}]^T$ [43], where the all-zero matrix $\mathbf{0}$ has $[M \times (T - M)]$ elements.

TABLE I: Summary of the DSTM schemes.

| | Transmitter complexity | | Receiver complexity | | Performance | |
|---|---|---|---|---|---|---|
| | Finite-cardinality? | Single-RF transmission? | Single-stream ML detection? | Detection complexity order | Transmit diversity? | Diversity gain maximization? |
| DSTBC [4]–[6] | × | × | √ | $\mathcal{O}(Q)$ | √ | × |
| DLDC [12], [13] | × | × | × | $\mathcal{O}(I = 2^{RT})$ | √ | √ |
| DSTSK [14]–[16] | × | × | √ | $\mathcal{O}(Q)$ | √ | √ |
| DGC [39], [41]–[43] | √ | √ | × | $\mathcal{O}(I = 2^{RT})$ | √ | √ |
| DSM [31]–[34] | √ | √ | √ | $\mathcal{O}(2^{\lfloor \log_2 T! \rfloor})$ | × | × |
| FE-DSM [37], [38] | √ | √ | √ | $\mathcal{O}(T)$ | √ | × |
| DSTBC-ISK [40] | √ | √ | √ | $\mathcal{O}(T)$ | √ | × |
| DSTSK-DAST | √ | √ | √ | $\mathcal{O}(Q)$ | √ | √ |
| DSTSK-TAST | √ | √ | √ | $\mathcal{O}(QT)$ | √ | √ |

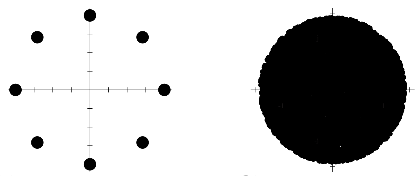

(a) Constellation for $\mathbf{X}$ (b) Constellation for $\mathbf{S}$

Fig. 1: Constellations of DSTBC [6] signals in $\mathbf{X}$ and $\mathbf{S}$ of (1), where $M = 2$ TAs and 8PSK signals are used.

The data-signal matrix $\mathbf{X}_{n-1}$ of (1) may invoke any unitary MIMO signal structures including STBC, STSK and Cayley transformed LDC, which form the DSTM schemes of DSTBC [4]–[6], DSTSK [14]–[16] and DLDC [12], [13], respectively. However, when coherent MIMO signals are directly used in DSTM, the matrix multiplication of (1) typically results in arbitrary transmitted signals having a cardinality tending to infinity. This problem is exemplied for the case of DSTBC [6] in Fig. 1. Although the differential design aims for a low transceiver complexity, compared to the coherent STBC, the DSTBC's infinite-cardinality problem actually imposes significantly extra constraints on the speed, precision and power consumption of both the digital circuitry and on the Digital-to-Analog Converter (DAC). Moreover, when the DSTBC signals of Fig. 1(b) are quantized to a finite-cardinality set, the associated quantization error results in a severe performance loss, as demonstrated in [40]. As a remedy, the finite-cardinality design of DSM [31]–[34], FE-DSM [37], [38], DSTBC-ISK [40] and DGC [39], [41]–[43] confines the signal matrix $\mathbf{X}_{n-1}$ of (1) to have only a single non-zero element in each row and column, where the non-zero signal is drawn from the equi-spaced PSK and star QAM constellations. As a further benefit of using the sparse matrix, only a single RF chain is activated for signal transmission.

We note that a single-carrier system is assumed in this paper, owing to the fact that the single-RF feature cannot be retained by Orthogonal Frequency-Division Multiplexing (OFDM) [44]. Nonetheless, considering that the products of the communication industry are typically standardized, our main objective of preserving the finite-cardinality feature also offers a practical interface to OFDM applications, where the DSTM signals in $\mathbf{S}_n$ may be fed into the Inverse Discrete Fourier Transform (IDFT) block as the frequency-domain input signals. More explicitly, the frequency-domain signals entered into the IDFT block at the OFDM transmitter are generally drawn from the standardized finite-cardinality PSK/QAM constellations. In particular, a variety of practical techniques - including active constellation extension, selected mapping, tone injection and tone reservation [45]–[48] - explicitly aim for the OFDM time-domain signal's Peak-to-Average Power Ratio (PAPR) reduction based on the frequency-domain input PSK/QAM constellations. Therefore, the finite-cardinality feature that retains the standardized PSK/QAM signal constellation is of practical importance to the applications both in single-carrier systems and in multi-carrier OFDM systems.

## B. Received Signal Model

In order to present a fair comparison against the existing finite-cardinality DSTM schemes of DSM [31]–[34], FE-DSM [37], [38], DSTBC-ISK [40] and DGC [39], [41]–[43], the same narrowband single-carrier model is invoked, where the received signals are given by:

$$\mathbf{Y}_n = \mathbf{S}_n \mathbf{H}_n + \mathbf{V}_n. \tag{2}$$

$\mathbf{Y}_n$, $\mathbf{H}_n$ and $\mathbf{V}_n$ are the $(T \times N)$-element received signal matrix, the $(M \times N)$-element Rayleigh fading channel matrix as well as the $(T \times N)$-element AWGN matrix, respectively. In quasi-static fading channels, we have $\mathbf{H}_n = \mathbf{H}_{n-1}$, hence (2) becomes $\mathbf{Y}_n = \mathbf{X}_{n-1}(\mathbf{Y}_{n-1} - \mathbf{V}_{n-1}) + \mathbf{V}_n$. This leads to the following differential detection:

$$\hat{\mathbf{X}}_{n-1} = \arg \min_{\forall \mathbf{X}^i} \left\| \mathbf{Y}_n - \mathbf{X}^i \mathbf{Y}_{n-1} \right\|^2, \tag{3}$$

which results in the following Pairwise Error Probability (PEP) [49], [50] for the case of $M = T$:

$$p(\mathbf{X}^i \to \mathbf{X}^{i'}) \leq \left\{ 1 + \left[\frac{1}{4N_0(N_0+2)}\right]^{\text{rank}(\boldsymbol{\Delta})} \det(\boldsymbol{\Delta}) + \frac{1}{4N_0(N_0+2)} \text{tr}(\boldsymbol{\Delta}) \right\}^{-N}, \tag{4}$$

where the determinant $\det(\boldsymbol{\Delta}) = \prod_{t=1}^{T} \lambda_t$ and the trace term $\text{tr}(\boldsymbol{\Delta}) = \sum_{t=1}^{T} \lambda_t$ dominates the PEP in the high- and low-SNR regions, respectively, while $\{\lambda_t\}_{t=1}^{T}$ are eigenvalues of $\boldsymbol{\Delta} = (\mathbf{X}^i - \mathbf{X}^{i'})^H (\mathbf{X}^i - \mathbf{X}^{i'})$. Accordingly, the trend of (4) may be characterized by the *diversity product* and by the *diversity sum* as [50]:

$$\Lambda_p = \frac{1}{2} \min_{\forall i \neq i'} \det(\boldsymbol{\Delta})^{\frac{1}{2T}}. \tag{5a}$$

$$\Lambda_s = \frac{1}{2\sqrt{T}} \min_{\forall i \neq i'} \text{tr}(\boldsymbol{\Delta})^{\frac{1}{2}}. \tag{5b}$$

The tradeoff between $\Lambda_p$ and $\Lambda_s$ explicitly characterizes the ubiquitous diversity-throughput tradeoff in MIMO design, which is exemplied in Fig. 2. Detailed introductions to DGC and DSM will be offered in Sec. II-C and Sec. II-D, respectively. It is demonstrated by Fig. 2 that on one hand, the DGC-cyclic associated with the maximized $\Lambda_p = 0.3827$ achieves substantial diversity gains for $N = \{1, 2\}$, but it does not perform well for large $N = \{8, 16\}$. On the other

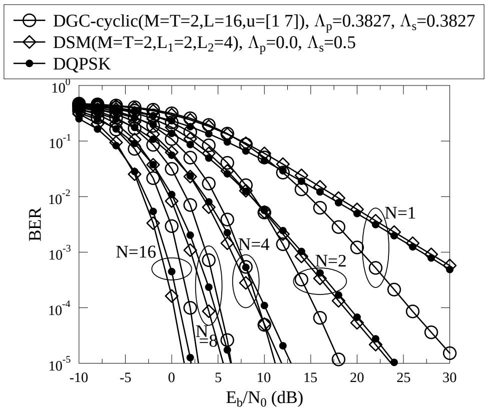


Fig. 2: BER performance comparison between DGC and DSM associated with $M = T = 2$ and $R = 2.0$.

TABLE II: Example of DGC-cyclic ($M = T = 2$, $L = 8$) at $R = 1.5$.

| | | | |
|---|---|---|---|
| $\mathbf{X}^0=\begin{bmatrix}1&0\\0&1\end{bmatrix}$, | $\mathbf{X}^1=\begin{bmatrix}w_8&0\\0&w_8^3\end{bmatrix}$, | $\mathbf{X}^2=\begin{bmatrix}w_8^2&0\\0&w_8^6\end{bmatrix}$, | $\mathbf{X}^3=\begin{bmatrix}w_8^3&0\\0&w_8^1\end{bmatrix}$, |
| $\mathbf{X}^4=\begin{bmatrix}w_8^4&0\\0&w_8^4\end{bmatrix}$, | $\mathbf{X}^5=\begin{bmatrix}w_8^5&0\\0&w_8^7\end{bmatrix}$, | $\mathbf{X}^6=\begin{bmatrix}w_8^6&0\\0&w_8^2\end{bmatrix}$, | $\mathbf{X}^7=\begin{bmatrix}w_8^7&0\\0&w_8^5\end{bmatrix}$ |

hand, the DSM associated with $\Lambda_p = 0$ performs even worse than its SISO DPSK counterpart for $N = 1$ in Fig. 2, but the DSM outperforms both DGC-cyclic and DPSK for large $N = \{8, 16\}$. This is because the DSM's throughput of $R = \frac{\lfloor \log_2 T! \rfloor + T \log_2 L}{T}$ is higher than the DPSK's $R = \log_2 L$ and the DGC-cyclic's $R = \frac{\log_2 L}{T}$. As a result, upon comparing the performance at the same throughput, the DSM may opt for a lower-level $L$PSK associated with a higher Euclidean distance, which leads to a higher $\Lambda_s$ of (5b) and hence a better performance for large $N$.

Essentially, all operational and future wireless communication systems are adaptive. For instance, the low-complexity transceiver of SM and DSM schemes is favourable for the evolving Internet-of-Things (IoT) in next generation networks. For the billions of connected smart devices, it is especially beneficial to adaptively switch between high-diversity and high-throughput schemes according to the specific service demands and link qualities. Therefore, in this work, we aim for devising new DSTM scheme that is capable of even outperforming the classic DGC, which mitigates the problem of the diminishing diversity gain of the recently developed FE-DSM and DSTBC-ISK, without compromising the DSM's appealingly low transceiver complexity.

### *C. Differential Group Code (DGC) Diversity Gain Maximization*

For cyclic DGCs [39], [41]–[43], the signal-matrix $\mathbf{X}$ of (1) is constructed by $\mathbf{X}^l = \mathbf{G}_c^l$, where $\mathbf{G}_c = \text{diag}([w_L^{u_1}, w_L^{u_2}, \cdots, w_L^{u_T}])$ and we have $w_L = \exp(j\frac{2\pi}{L})$. The integer phase-rotation parameters $\mathbf{u} = [u_1, u_2, \cdots, u_T]$ are chosen for the sake of maximizing the diversity product of $\Lambda_p = \min_{l \neq 0} [\prod_{t=1}^{T} |\sin(\frac{\pi u_t l}{L})|]^{\frac{1}{T}}$. Moreover, the dicyclic DGCs [39], [41]–[43] convey an extra bit determining whether the signal matrix is diagonal or anti-diagonal. It is shown in [39], [43] that DGC-cyclic generally outperform DGC-dicyclic.

Given a MIMO system setup, the DGC-cyclic strives for actively maximizing its diversity product of $\Lambda_p = \min_{l \neq 0} [\prod_{t=1}^{T} |\sin(\frac{\pi u_t l}{L})|]^{\frac{1}{T}}$ by searching for the best combination of $\{1 \leq u_t \leq L-1\}_{t=1}^{T}$. This exhaustive search is simplied in [42] as: (a) $\{u_t\}_{t=1}^{T}$ are relatively prime to $L$. Otherwise, we have $[u_t l \mod L = 0]$ that results in $\Lambda_p = 0$; (b) The ordering of $\{u_t\}_{t=1}^{T}$ does not change $\Lambda_p$, hence we set $u_1 \leq u_2 \leq \cdots \leq u_T$; (c) $u_t$ and $(L_{DM} - u_t)$ leads to the same $\Lambda_p$, which results in a reduced range of $\{1 \leq u_t \leq L/2 - 1\}_{t=1}^{T}$; (d) $u_1 = 1$ is set, because of rule (c) and also because multiplying $\{u_t\}_{t=2}^{T}$ by a common integer does not change $\Lambda_p$.

***Example 1:*** For a DGC-cyclic scheme associated with $M = T = 2$ and $L = 8$, the legitimate parameters according to the above search rules are given by $\mathbf{u} = [1, 1]$ and $\mathbf{u} = [1, 3]$, which lead to $\Lambda_p = 0.3827$ and $\Lambda_p = 0.5946$, respectively. Therefore, the latter is chosen, and the resultant signal matrices are given by $\{\mathbf{X}^l = \text{diag}([w_8^l, w_8^{3l}])\}_{l=0}^{7}$, which are detailed in Table II.

***Example 2:*** For DGC-cyclic associated with $M = T = 4$ and $L = 32$, there are a total of 120 candidates for $\mathbf{u}$ ranging from $\mathbf{u} = [1, 1, 1, 1]$ to $\mathbf{u} = [1, 15, 15, 15]$ according to the above search rules. The maximized $\Lambda_p = 0.3827$ is given by $u = [1, 7, 9, 15]$, which leads to the DGC signal matrices of $\{\mathbf{X}^l = \text{diag}([w_{32}^{l}, w_{32}^{7l}, w_{32}^{9l}, w_{32}^{15l}])\}_{l=0}^{31}$.

Owing to the non-linear phase rotations on the data-carrying $L$PSK signal, the DGC detection invoking (3) has a complexity order of $\mathcal{O}(I)$, which grows exponentially with the throughput.

### *D. Differential Spatial Modulation (DSM)*

The DSM [31]–[34] modulates a total of (M=T=Q) $\{L_t\}_{t=1}^{T}$-PSK symbols $\{x^{l_t} = \exp(j\frac{2\pi}{L_t}\check{l}_t)\}_{t=1}^{T}$ from a total of $\sum_{t=1}^{T} \log_2 L_t$ bits. Moreover, a total of $\lfloor \log_2 M! \rfloor = \log_2 \overline{M}$ bits are assigned for determining the activation sequence $\mathbf{a}_{\bar{m}} = [\mathrm{a}_{\bar{m},1}, \mathrm{a}_{\bar{m},2}, \cdots, \mathrm{a}_{\bar{m},T}]$, which obeys $1 \leq \{\mathrm{a}_{\bar{m},t}\}_{t=1}^{T} \leq M$ and $\mathrm{a}_{\bar{m},1} \neq \mathrm{a}_{\bar{m},2} \neq \cdots \neq \mathrm{a}_{\bar{m},T}$. The permutation index $\bar{m}$ ranges $1 \leq \bar{m} \leq \overline{M}$. This presentation indicates that the $\mathrm{a}_{\bar{m},t}$-th element on the $t$-th row of the $(T \times T)$-element data-carrying matrix $\mathbf{X}_{n-1}$ in (1) is activated to transmit $x^{l_t}$:

$$\mathbf{X}^i(r, c) = \begin{cases} x^{l_t}, & \text{if } r = t \text{ and } c = \mathrm{a}_{\bar{m},t} \\ 0, & \text{all the other elements} \end{cases}, \tag{6}$$

where $\mathbf{X}^i(r, c)$ denotes the element on the $r$-th row and $c$-th column in $\mathbf{X}^i$. The example of DSM associated with ($M = 2$) is characterized by Table III.

TABLE III: Example of DSM associated with $M = T = 2$

| Permutation Index | Activation Sequence | Data-Carrying Matrix |
|---|---|---|
| $\bar{m} = 1$ | $\mathbf{a}_1 = [1, 2]$ | $\mathbf{X}^{\{\bar{m}=1, l_1, l_2\}} = \begin{bmatrix} x^{l_1} & 0 \\ 0 & x^{l_2} \end{bmatrix}$ |
| $\bar{m} = 2$ | $\mathbf{a}_2 = [2, 1]$ | $\mathbf{X}^{\{\bar{m}=2, l_1, l_2\}} = \begin{bmatrix} 0 & x^{l_1} \\ x^{l_2} & 0 \end{bmatrix}$ |

Therefore, a pair of DSM codewords associated with $\bar{m} = \bar{m}'$, $l_1 = l_1'$ and $\{l_t \neq l_t'\}_{t=2}^{T}$ leads to $\Lambda_p = 0$ in (5a). Nonetheless, in the family of the existing finite-cardinality single-RF DSTM schemes, DSM offers the highest throughput of $R = \frac{\lfloor \log_2 T! \rfloor + T \log_2 L}{T}$, which is beneficial for using large $N$, as discussed in Sec. II-B. Moreover, we note that DSM may invoke the single-stream ML detector designed in Sec. IV of [40], which has a reduced complexity order of $\mathcal{O}(\overline{M})$.

## III. Differential Space-Time Shift Keying Using Diagonal Algebraic Space-Time (DSTSK-DAST)

In this section, we propose the new DSTSK-DAST scheme, which simultaneously achieves our design objectives of (1) forming a finite-cardinality set of transmitted signals, (2) retaining a single-stream ML detection complexity and (3) maximizing the diversity gain.

### A. The Relationship Between DAST and LDC

Before the development of space-time diversity for MIMO systems, the temporal diversity was imposed onto a sequence of $Q$ modulated symbols $\mathbf{x}=[x_1,\cdots,x_Q]^T$ in SISO systems by a series of $Q$ dispersion elements $\{\{\overline{a}_{t,q}\}_{t=1}^T\}_{q=1}^Q$ as $\overline{x}_t = \sum_{q=1}^Q \overline{a}_{t,q}x_q$. As a result, the receiver is capable of recovering the dispersed sequence of $T$ correlated symbols $\overline{\mathbf{x}}=[\overline{x}_1,\cdots,\overline{x}_T]^T$ unless the whole sequence experiences a deep fade. This SISO diversity design was termed as lattice-based multidimensional constellation [51]–[53], where the best rotations $\{\{\overline{a}_{t,q}\}_{t=1}^T\}_{q=1}^Q$ are obtained according to algebraic number theory. More explicitly, according to the construction based on PSK signalling in [51], the dispersed sequence may be represented by:

$$\overline{\mathbf{x}} = \mathbf{G}_A\mathbf{x}, \tag{7}$$

where $\mathbf{G}_A = \text{VDM}_{T\times Q}(g_1,\cdots,g_T)$ is a $(T\times Q)$-element Vandermonde matrix:

$$\begin{aligned}\mathbf{G}_A &= \begin{bmatrix} \overline{a}_{1,1} & \overline{a}_{1,2} & \overline{a}_{1,3} & \cdots & \overline{a}_{1,Q} \\ \overline{a}_{2,1} & \overline{a}_{2,2} & \overline{a}_{2,3} & \cdots & \overline{a}_{2,Q} \\ \vdots & \vdots & \vdots & \ddots & \vdots \\ \overline{a}_{T,1} & \overline{a}_{T,2} & \overline{a}_{T,3} & \cdots & \overline{a}_{T,Q}\end{bmatrix} \\ &= \begin{bmatrix} 1 & g_1 & g_1^2 & \cdots & g_1^{Q-1} \\ 1 & g_2 & g_2^2 & \cdots & g_2^{Q-1} \\ \vdots & \vdots & \vdots & \ddots & \vdots \\ 1 & g_T & g_T^2 & \cdots & g_T^{Q-1}\end{bmatrix}.\end{aligned} \tag{8}$$

Therefore, the diversity is imposed by the spreading operation of $\overline{x}_t = \sum_{q=1}^Q \overline{a}_{t,q}x_q = \sum_{q=1}^Q g_t^{q-1}x_q$, where $\{g_t\}_{t=1}^T$ are taken from a $4T$-PSK constellation according to [51].

In order to achieve the space-time diversity in MIMO systems, the DAST scheme in [7] proposed to transmit the dispersed sequence of $\overline{\mathbf{x}}$ on diagonal of the MIMO's space-time signal matrix. More explicitly, DAST using PSK may be constructed by:

$$\begin{aligned}\mathbf{X} &= \text{diag}(\mathbf{G}_A\mathbf{x}) \\ &= \text{diag}\left(\left[\sum_{q=1}^Q g_1^{q-1}x_q, \sum_{q=1}^Q g_2^{q-1}x_q, \cdots, \sum_{q=1}^Q g_T^{q-1}x_q\right]\right).\end{aligned} \tag{9}$$

As a result, the DAST signal matrix of (9) may be further expressed in the LDC form [9] as:

$$\mathbf{X} = \sum_{q=1}^Q x_q\mathbf{A}_q, \tag{10}$$

where we have the equivalent LDC dispersion matrices of $\{\mathbf{A}_q = \text{diag}([g_1^{q-1},\cdots,g_T^{q-1}])\}_{q=1}^Q$, while $Q=T$ is assumed for the DAST scheme in [7].

Although both $\{g_t\}_{t=1}^T$ and $\{x_q\}_{q=1}^Q$ are PSK signals, the dispersed symbols $\{\overline{x}_t = \sum_{q=1}^Q g_t^{q-1}x_q\}_{t=1}^T$ do not remain limited to the PSK constellation owing to the additions of "$\sum_{q=1}^Q$". Consequently, when the signal matrix of (10) is invoked in the differential encoding of (1), the infinite-cardinality problem discussed in Sec. II-A arises. Moreover, we note that the DAST's signal matrix of (10) is not unitrary, which prevents the employment of a single-stream ML detector.

TABLE IV: Examples of DGC-cyclic and DSTSK-DAST associated with $M=T=4$.

| DGC-cyclic | DSTSK-DAST |
|---|---|
| $\mathbf{X}^l=\mathbf{G}_c^l=\begin{bmatrix} w_L^{u_1} & 0 & 0 & 0 \\ 0 & w_L^{u_2} & 0 & 0 \\ 0 & 0 & w_L^{u_3} & 0 \\ 0 & 0 & 0 & w_L^{u_4}\end{bmatrix}^l$ | $\mathbf{X}^i=x^l\mathbf{A}_q=w_L^l\begin{bmatrix} w_{L_{DM}}^{u_1} & 0 & 0 & 0 \\ 0 & w_{L_{DM}}^{u_2} & 0 & 0 \\ 0 & 0 & w_{L_{DM}}^{u_3} & 0 \\ 0 & 0 & 0 & w_{L_{DM}}^{u_4}\end{bmatrix}^q$ |

### B. Finite-Cardinality Design

In order to conceive a finite-cardinality DSTSK-DAST scheme, we revise the LDC's matrix multiplexing form of (10) to the STSK's matrix activation form [14] as:

$$\mathbf{X} = x^l\mathbf{A}_q. \tag{11}$$

More explicitly, a total of $\log_2 L$ bits are assigned to modulate a $L$-PSK symbol $\{x^l = w_L^l\}_{l=0}^{L-1}$, and a total of $\log_2 Q$ bits are assigned to activate a single out of $Q$ dispersion matrix $\mathbf{A}_q$. The dispersion matrices are given by $\{\mathbf{A}_q = \text{diag}([w_{L_{DM}}^{(q-1)u_1}, w_{L_{DM}}^{(q-1)u_2},\cdots,w_{L_{DM}}^{(q-1)u_T}])\}_{q=1}^Q$, where the dispersion elements are taken from an $L_{DM}$-PSK constellation. The sequence of integers $\mathbf{u}=[u_1,u_2,\cdots,u_T]$ are invoked for the sake of diversity gain maximization in the same way as the DGC, which will be further detailed in Sec. III-D.

The revised signal matrix of (11) is equivalent to the DAST of (9), where the $(T\times Q)$-element Vandermonde matrix $\mathbf{G}_A$ is now given by:

$$\begin{aligned}\mathbf{G}_A &= \text{VDM}_{T\times Q}(w_{L_{DM}}^{u_1},\cdots,w_{L_{DM}}^{u_T}) \\ &= \begin{bmatrix} 1 & w_{L_{DM}}^{u_1} & w_{L_{DM}}^{2u_1} & \cdots & w_{L_{DM}}^{(Q-1)u_1} \\ 1 & w_{L_{DM}}^{u_2} & w_{L_{DM}}^{2u_2} & \cdots & w_{L_{DM}}^{(Q-1)u_2} \\ \vdots & \vdots & \vdots & \ddots & \vdots \\ 1 & w_{L_{DM}}^{u_T} & w_{L_{DM}}^{2u_T} & \cdots & w_{L_{DM}}^{(Q-1)u_T}\end{bmatrix},\end{aligned} \tag{12}$$

and the $Q$-element signal vector $\mathbf{x}$ is now given by:

$$\mathbf{x} = [\underbrace{0\ \cdots\ 0}_{q-1}, x^l, \underbrace{0\ \cdots\ 0}_{Q-q}]. \tag{13}$$

Therefore, in the absence of signal additions, the DSTSK-DAST signal matrix of (11) complies with the finite-cardinality design of Sec. II-A. We note that (11) requires $L_{DM}\geq LQ$ for creating distinct codewords $\{\mathbf{X}^i\}_{i=0}^I$. We opt for choosing $L_{DM}=LQ$ for the sake of simplicity. Moreover, for the proposed DSTSK-DAST, $Q$ and $T$ do not have to be equal, hence the throughput is now given by $R=\frac{\log_2 L+\log_2 Q}{T}$.

### C. Single-Stream ML Detection

The relationship between DGC-cyclic and DSTSK-DAST is further exemplied in Table IV, which demonstrates that instead of directly rotating the data-carrying $L$PSK signal, the DSTSK-DAST applies the phase-rotation parameters of $\mathbf{u} = [u_1, u_2, \cdots, u_T]$ to the $L_{DM}$PSK signals in the dispersion matrix. As a result, the detection of (3) may be decoupled for the DSTSK-DAST as:

$$\hat{\mathbf{X}}_{n-1} = \arg \max_{\forall \mathbf{X}_{n-1}} \Re \left[ \text{tr} \left( \mathbf{X}_{n-1}^H \mathbf{Z} \right) \right] = \arg \max_{\forall q,l} \Re \left[ (x^l)^* \widetilde{z}_q \right]. \tag{14}$$

We have $\mathbf{Z} = \mathbf{Y}_n \mathbf{Y}_{n-1}^H$ and $\widetilde{z}_q = \text{tr}\left( \overline{\mathbf{A}}_q^H \mathbf{Z} \right) = \sum_{t=1}^T w_{L_{DM}}^{-(q-1)u_t} z_{t,t}$, where $z_{t,t}$ denotes the element on the $t$-th row and $t$-th column in $\mathbf{Z}$. As a result, the single-stream $L$-PSK demodulator $\mathbb{M}_{\text{PSK}}^{-1}(\cdot)$ may be invoked a total of $Q$ times for all indices $q$ as:

$$\hat{l}_q = \mathbb{M}_{\text{PSK}}^{-1}(\widetilde{z}_q), \tag{15}$$

where the phase of $\widetilde{z}_q$ may be directly rounded[1] as $\check{l}_q = \lfloor \frac{L}{2\pi} \angle \widetilde{z}_q \rceil$. Following this, the optimum activation index may be detected by invoking (14) for a reduced number of $Q$ times as:

$$\hat{q} = \arg \max_{\forall q} \Re \left[ (x^{\hat{l}_q})^* \widetilde{z}_q \right]. \tag{16}$$

Finally, the optimum $L$-PSK index is $\hat{l} = \hat{l}_{\hat{q}}$, which is the one obtained in (15) associated with $\hat{q}$ of (16). In summary, the DSTSK-DAST's single-stream-based ML detection complexity order is given by $\mathcal{O}(Q)$, which does not grow with the $L$-PSK constellation size.

### D. Diversity Gain Maximization

In order to simplify the parameter search, let us firstly introduce the following proposition for the simplified evaluation of the DSTSK-DAST's diversity product:

***Proposition 1:*** The DSTSK-DAST's diversity product of (5a) is given by

$$\Lambda_p = \min_{\forall (l \neq 0 || q \neq 1)} \prod_{t=1}^T \left| \sin \left[ \frac{\pi (q u_t - u_t + l L_{DM}/L)}{L_{DM}} \right] \right|^{1/T}. \tag{17}$$

*Proof.* Owing to the fact that DSTSK-DAST's signal matrices of (11) form a finite group under multiplication [39], [41]–[43], the determinant term in (5a) may be further expressed as:

$$\begin{aligned} \det(\mathbf{\Delta}) &= \det \left[ (\mathbf{I}_T - x^l \mathbf{A}_q)^H (\mathbf{I}_T - x^l \mathbf{A}_q) \right] \\ &= \prod_{t=1}^T \left| 1 - w_L^l w_{L_{DM}}^{(q-1)u_t} \right|^2 \\ &= \prod_{t=1}^T \left| 1 - \exp \left\{ \frac{2\pi[(q-1)u_t + l L_{DM}/L]}{L_{DM}} \right\} \right|^2, \end{aligned} \tag{18}$$

which results in (17) according to the relationship of $|1 - \exp(j\theta)|^2 = 4 \sin^2 \frac{\theta}{2}$. $\square$

As a result, with given a MIMO system setup, the DSTSK-DAST may also actively maximize $\Lambda_p$ of (17) by searching over all the possible combinations of $\{1 \leq u_t \leq L_{DM} - 1\}_{t=1}^T$. The search space may be further reduced according to:

[1] We note that the detected index $\hat{l}$ recovers the $L$PSK index $l$ that can be translated back to source bits as $\text{dec2bin}(l) = (b_1 \cdots b_{\log_2 L})$. Moreover, $l$ is the Gray coded version of the natural index $\check{l}$ as defined in the $L$PSK modulation of $x^l = \exp(\frac{2\pi}{L} \check{l})$.

TABLE V: Example of DSTSK-DAST($M = T = 2$) using $Q = 2$, $L = 4$, $L_{DM} = 8$ and $\mathbf{u} = [1, 5]$ at $R = 1.5$.

| Input bits | PSK symbol | Dispersion matrix | Data-carrying matrix |
|---|---|---|---|
| 000 | $x^0 = 1$ | $\mathbf{A}_1 = \begin{bmatrix} 1 & 0 \\ 0 & 1 \end{bmatrix}$ | $\mathbf{X}=x^0\mathbf{A}_1=\begin{bmatrix} 1 & 0 \\ 0 & 1 \end{bmatrix}$ |
| 001 | $x^0 = 1$ | $\mathbf{A}_2 = \begin{bmatrix} w_8 & 0 \\ 0 & w_8^5 \end{bmatrix}$ | $\mathbf{X}=x^0\mathbf{A}_2=\begin{bmatrix} w_8 & 0 \\ 0 & w_8^5 \end{bmatrix}$ |
| 010 | $x^1 = j$ | $\mathbf{A}_1 = \begin{bmatrix} 1 & 0 \\ 0 & 1 \end{bmatrix}$ | $\mathbf{X}=x^1\mathbf{A}_1=\begin{bmatrix} w_8^2 & 0 \\ 0 & w_8^2 \end{bmatrix}$ |
| 011 | $x^1 = j$ | $\mathbf{A}_2 = \begin{bmatrix} w_8 & 0 \\ 0 & w_8^5 \end{bmatrix}$ | $\mathbf{X}=x^1\mathbf{A}_2=\begin{bmatrix} w_8^3 & 0 \\ 0 & w_8^7 \end{bmatrix}$ |
| 100 | $x^2 = -j$ | $\mathbf{A}_1 = \begin{bmatrix} 1 & 0 \\ 0 & 1 \end{bmatrix}$ | $\mathbf{X}=x^2\mathbf{A}_1=\begin{bmatrix} w_8^6 & 0 \\ 0 & w_8^6 \end{bmatrix}$ |
| 101 | $x^2 = -j$ | $\mathbf{A}_2 = \begin{bmatrix} w_8 & 0 \\ 0 & w_8^5 \end{bmatrix}$ | $\mathbf{X}=x^2\mathbf{A}_2=\begin{bmatrix} w_8^7 & 0 \\ 0 & w_8^3 \end{bmatrix}$ |
| 110 | $x^3 = -1$ | $\mathbf{A}_1 = \begin{bmatrix} 1 & 0 \\ 0 & 1 \end{bmatrix}$ | $\mathbf{X}=x^3\mathbf{A}_1=\begin{bmatrix} w_8^4 & 0 \\ 0 & w_8^4 \end{bmatrix}$ |
| 111 | $x^3 = -1$ | $\mathbf{A}_2 = \begin{bmatrix} w_8 & 0 \\ 0 & w_8^5 \end{bmatrix}$ | $\mathbf{X}=x^3\mathbf{A}_2=\begin{bmatrix} w_8^5 & 0 \\ 0 & w_8 \end{bmatrix}$ |

(a) $\{u_t\}_{t=1}^T$ are relatively prime to $L_{DM}$. Otherwise, there exists $[u_t(q-1) \bmod L_{DM} = 0]$ for some integer $q$, which results in $\Lambda_p = 0$ in (17).

(b) The ordering of $\{u_t\}_{t=1}^T$ does not change $\Lambda_p$, hence we set $u_1 \leq u_2 \leq \cdots \leq u_T$.

We note that unlike DGC of Sec. II-C, $u_t$ and $(L_{DM} - u_t)$ are no longer equivalent in (17). In summary, the resultant search space is bounded by a total of $[(\frac{L_{DM}}{2})^T/2 + (\frac{L_{DM}}{2})^{T/2}/2]$ combinations for $\{u_t\}_{t=1}^T$.

The brute-force exhaustive search constitutes a better choice than random search [8], [9], [14] or the classic gradient-ascent based search [12], [54], [55], because the cost function of (17) is not concave. Nonetheless, when the search space becomes excessive as $Q$ and $L$ increase, we may still resort to random search, since the optimization of (17) is no longer sensitive to its values at a high throughput. As a further benefit, instead of storing the dispersion matrices at the conventional DSTSK transmitters [14]–[16], the DSTSK-DAST transmitter only has to store the $T$-element integer phase-rotation parameters $\mathbf{u} = [u_1, \cdots, u_T]$.

***Example 3:*** Let us consider the DSTSK-DAST using $M = T = 2$ at the throughput of $R = \frac{\log_2 LQ}{T} = 1.5$, where we have $L_{DM} = LQ = 8$. Considering that the DSTSK-DAST detection complexity order in Sec. III-C is given by $\mathcal{O}(Q)$, we commence from the parameter combination of $Q = 1$ and $L = 8$. The exhaustive search gives $\mathbf{u} = [1, 1]$ associated with the diversity product of $\Lambda_p = 0.3827$, which is still smaller than the $\Lambda_p = 0.5946$ value of its DGC counterpart in Example 1. Therefore, we further increase $Q$ and use the updated combination of $Q = 2$ and $L = 4$. The exhaustive search gives $\mathbf{u} = [1, 5]$ achieving $\Lambda_p = 0.5946$. The corresponding signal matrices are summarized in Table V. The resultant DSTSK-DAST detection complexity order is $\mathcal{O}(Q = 2)$, which is substantially lower than the full-search based DGC detection complexity order of $\mathcal{O}(I = 8)$ in Example 1, despite the fact that both DSTSK-DAST and DGC achieve the same maximized diversity product of $\Lambda_p = 0.5946$.

***Example 4:*** For a DSTSK-DAST using $M = T = 4$ at $R = 1.25$, following the same procedures as Example 3, we arrive at the parameters of $Q = 4$, $L = 8$, $L_{DM} = 32$ and $\mathbf{u} = [7, 15, 23, 31]$, which achieves the same $\Lambda_p = 0.3827$ as the DGC in Example 2. The resultant DSTSK-DAST signal matrices are given by $\{\{\mathbf{X}^i =$

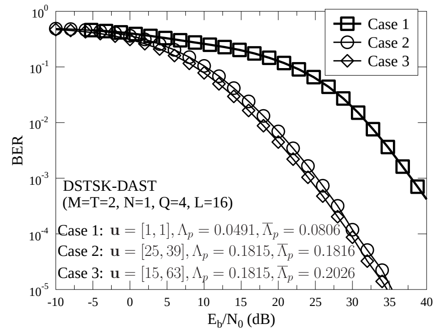


Fig. 3: Performance of DSTSK-DAST($M = T = 2$, $N = 1$, $Q = 4$, $L = 16$) associated with different $\mathbf{u}$.

$w_8^l \mathbf{A}_q\}_{l=0}^7\}_{q=1}^4$, where the dispersion matrices are given by $\{\mathbf{A}_q = \text{diag}([w_{32}^{7(q-1)}, w_{32}^{15(q-1)}, w_{32}^{23(q-1)}, w_{32}^{31(q-1)}])\}_{q=1}^Q$. Similarly, the resultant DSTSK-DAST detection complexity order of $\mathcal{O}(Q = 4)$ is substantially lower than the DGC complexity order of $\mathcal{O}(I = 32)$ in Example 2.

### *E. Further Considerations Concerning Average BER*

It was demonstrated in [54] that the diversity product $\Lambda_p$ of (5a) that characterizes the worst PEP $p(\mathbf{X}^i \to \mathbf{X}^{i'})$ of (4) does not always reflect the trend of the averaged BER:

$$\overline{P}_{e,bit} \leq \text{ E}\left\{\sum_{i=0}^{I-1}\sum_{i'=0}^{I-1}\frac{d_H(i,i')}{I\log_2 I}p(\mathbf{X}^i \to \mathbf{X}^{i'})\right\}, \quad (19)$$

where $d_H(i, i')$ refers to the Hamming distance between the bit-mappings of $\mathbf{X}^i$ and $\mathbf{X}^{i'}$. Against this background, the *average diversity product* was conceived based on (19) in [40] as:

$$\overline{\Lambda}_p = \frac{1}{2}\left(\frac{2}{\log_2 I+1}\sum_{\forall i}\sum_{\forall i'\neq i}\frac{d_H(i,i')}{I\log_2 I\det(\mathbf{\Delta})}\right)^{-\frac{1}{2T}}. \quad (20)$$

The performance results of DSTSK-DAST($M = T = 2$, $Q = 4$, $L = 16$) associated with different $\Lambda_p$ and $\overline{\Lambda}_p$ are exemplied in Fig. 3, which demonstrates that when both $\mathbf{u} = [25, 39]$ and $\mathbf{u} = [15, 63]$ achieve the maximum of $\Lambda_p = 0.1815$, the latter choice associated with a higher $\overline{\Lambda}_p = 0.2026$ exhibits a better performance. *Therefore, we propose to use* $\overline{\Lambda}_p$ *of* (20) *as the secondary objective function for all diversity-gain-maximizing DSTM schemes.* Explicitly, when several candidates $\mathbf{u}$ achieve the same maximum $\Lambda_p$, the one associated with the highest $\overline{\Lambda}_p$ is chosen.

## IV. Differential Space-Time Shift Keying Using Threaded Algebraic Space-Time (DSTSK-TAST)

In order to achieve a further improved performance, we propose a new DSTSK-TAST. More explicitly, we firstly represent the TAST [10] in the LDC form in Sec. IV-A, and then transform it into the STSK form in Sec. IV-B. The resultant finite-cardinality DSTSK-TAST invokes the single-stream DSTSK detectors in Sec. IV-C, and its diversity gain is maximized in Sec. IV-D. Finally, the diversity product of the proposed DSTSK-TAST is compared to the existing diversity-oriented finite-cardinality DSTM schemes in Sec. IV-E.

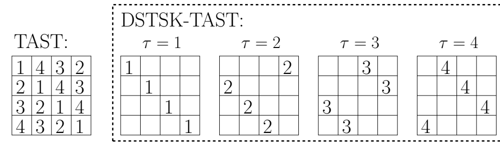


Fig. 4: Examples of TAST signal matrix [10] and DSTSK-TAST signal matrix for $M = T = 4$.

### *A. The Relationship Between TAST and LDC*

Instead of only using the diagonal matrix, the TAST in [10] divides a $(T \times T)$-element space-time matrix into $T$ non-overlapping threaded layers, where each threaded layer transmits a dispersed sequence $\overline{\mathbf{x}}_\tau = \{\mathbf{G}_A\mathbf{x}_\tau\}_{\tau=1}^T$. An example of the TAST matrix associated with $(T = 4)$ is portrayed in Fig. 4. More explicitly, for the PSK signalling, the TAST is constructed by [10]:

$$\mathbf{X} = \sum_{\tau=1}^T \phi_r^{\tau-1}\text{diag}(\mathbf{G}_A\mathbf{x}_\tau)\mathbf{G}_r^{\tau-1}, \quad (21)$$

where the phase rotations $\{\phi_r^{\tau-1} = w_{L_r}^{\tau-1}\}_{\tau=1}^T$ are taken from a $L_r$-PSK constellation, which are invoked for the sake of retaining the full diversity order. The dispersion-element generator matrix $\mathbf{G}_A$ is given by (8). Moreover, the layer-swithing generator matrix $\mathbf{G}_r$ is given by:

$$\mathbf{G}_r = \begin{bmatrix} 0 & \cdots & 0 & 1 \\ 1 & \cdots & 0 & 0 \\ \vdots & \ddots & \vdots & \vdots \\ 0 & \cdots & 1 & 0 \end{bmatrix}. \quad (22)$$

Similar to the DAST of (10), the TAST of (21) may also be expressed in the form of LDC:

$$\mathbf{X} = \sum_{\tau=1}^T\sum_{q=1}^Q x_{\tau,q}\mathbf{A}_{\tau,q}, \quad (23)$$

where the dispersion matrices are $\{\{\mathbf{A}_{\tau,q} = \phi_r^{\tau-1}\text{diag}([g_1^{q-1}, \cdots, g_T^{q-1}])\mathbf{G}_r^{\tau-1}\}_{\tau=1}^T\}_{q=1}^Q$, while the TAST in [10] assumes $Q = T$.

### *B. Finite-Cardinality Design*

For the sake of forming a finite-cardinality signals set, we now propose the DSTSK-TAST, which revises the LDC's multiplexing form of (23) to the STSK's activation form [14]:

$$\mathbf{X} = x^l\mathbf{A}_{\tau,q}, \quad (24)$$

where $\log_2 L$, $\log_2 T$ and $\log_2 Q$ number of bits are separately assigned to the $L$-PSK index $l$, the layer activation index $\tau$ and the dispersion activation index $q$, respectively. Based on the DSTSK-DAST design of (11), the dispersion matrices in (24) are now given by $\{\{\mathbf{A}_{\tau,q} = \phi_r^{\tau-1}\text{diag}([w_{L_{DM}}^{(q-1)u_1}, \cdots, w_{L_{DM}}^{(q-1)u_T}])\mathbf{G}_r^{\tau-1}\}_{\tau=1}^T\}_{q=1}^Q$. Therefore, the throughput of DSTSK-TAST is $R = \frac{\log_2 L+\log_2 Q+\log_2 T}{T}$, where $\log_2 T$ extra bits are conveyed compared to DSTSK-DAST.

Moreover, (24) requires that $L_r \geq \max\{LT, LQ, L_{DM}\}$ for creating distinct codewords. Once again, for the sake of simplicity, we generally choose $L_{DM} = LQ$ and $L_r = \max\{LT, L_{DM}\}$.

### C. Single-Stream ML Detection

Similar to DSTSK-DAST, the ML detection of (3) may be decoupled for DSTSK-TAST as $\hat{\mathbf{X}}_{n-1} = \arg\ \max_{\forall\tau,q,l} \Re\left[(x^l)^* \widetilde{z}_{\tau,q}\right]$, where we have $\widetilde{z}_{\tau,q} = \text{tr}\left(\overline{\mathbf{A}}_{\tau,q}^H \mathbf{Z}\right)$, which may be further simplied as $\widetilde{z}_{\tau,q} = (\phi_r^{\tau-1})^* \sum_{t=1}^{T} w_{L_{DM}}^{-(q-1)u_{\bar{t}}} z_{\bar{t},t}$ associated with $\bar{t} = \{[T+(t-1)-(\bar{\tau}-1)] \bmod T\}+1$ and $\bar{\tau} = \{[T-(\tau-1)] \bmod T\}+1$. As a result, the $L$-PSK demodulator is invoked $TQ$ times as $\{\{\hat{l}_{\tau,q} = \mathbb{M}_{\text{PSK}}^{-1}(\widetilde{z}_{\tau,q})\}_{\tau=1}^{T}\}_{q=1}^{Q}$. Then the optimum activation indices may be detected as $(\hat{\tau},\hat{q}) = \arg\ \max_{\forall\tau,q} \Re\left[(x^{\hat{l}_{\tau,q}})^* \widetilde{z}_{\tau,q}\right]$. Finally, the optimum $L$-PSK index is directly given by $\hat{l} = \hat{l}_{\hat{\tau},\hat{q}}$. In summary, the DSTSK-TAST's single-stream ML detection complexity order is given by $\mathcal{O}(TQ)$.

### D. Diversity Gain Maximization

Since DSTSK-TAST forms a finite group, its diversity product of (5a) may be expressed as:

$$\Lambda_p = \frac{1}{2} \min_{\forall i \neq 0}\ \det\left[(\mathbf{I}_T - x^l \mathbf{A}_{\tau,q})^H (\mathbf{I}_T - x^l \mathbf{A}_{\tau,q})\right]^{\frac{1}{2T}}. \quad (25)$$

It becomes more difficult to further simplify (25) because of the associated layer-swithing. Nonetheless, we offer the following two propositions for the cases of $T = 2$ and $T = 4$:

***Proposition 2:*** For $T = 2$, the DSTSK-TAST's diversity product of (25) is given by:

$$\begin{aligned}
&\Lambda_p = \min_{\tau=\{1,2\}} \Lambda_p^{\tau}, \ \text{where} \\
&\Lambda_p^{\tau=1} = \min_{\forall(l\neq0||q\neq1)} \prod_{t=1}^{T} \left|\sin\left[\frac{\pi(qu_t - u_t + lL_{DM}/L)}{L_{DM}}\right]\right|^{\frac{1}{T}}, \\
&\Lambda_p^{\tau=2} = \min_{\forall l\forall q\forall(\tau\neq0)} \frac{\sqrt[T]{2}}{2} \left|\sin\left[\frac{(q-1)(\sum_{t=1}^{T} u_t)\pi}{L_{DM}} + \frac{T\pi l}{L} + \frac{T\pi(\tau-1)}{L_r}\right]\right|^{\frac{1}{T}}.
\end{aligned} \quad (26)$$

*Proof.* For the case of $\tau = 1$, DSTSK-TAST's signal matrix of (24) is the same as DSTSK-DAST of (11), hence $\Lambda_p^{\tau=1}$ of (26) is given by (17) in Proposition 1. For $\tau = 2$, the determinant term in (25) is further extended as:

$$\begin{aligned}
\det(\mathbf{\Delta}) &= 4 - |\phi_r^* w_{L_{DM}}^{-(q-1)u_1} w_L^{-l} + \phi_r w_{L_{DM}}^{(q-1)u_2} w_L^{l}|^2 \\
&= 4\sin^2\left[\frac{(q-1)(u_1+u_2)\pi}{L_{DM}} + \frac{2\pi l}{L} + \frac{2\pi(\tau-1)}{L_r}\right],
\end{aligned} \quad (27)$$

which results in $\Lambda_p^{\tau=2}$ of (26) associated with $T = 2$. □

***Proposition 3:*** For $T = 4$, the DSTSK-TAST's diversity product of (25) is given by $\Lambda_p = \min_{\tau=\{1,2,3\}} \Lambda_p^{\tau}$, where $\Lambda_p^{\tau=1}$ and $\Lambda_p^{\tau=2}$ are given by (26) associated with $T = 4$. Moreover, the third term $\Lambda_p^{\tau=3}$ is given by:

$$\begin{aligned}
\Lambda_p^{\tau=3} = &\frac{1}{\sqrt{2}} \left|\sin\left[\frac{(q-1)(u_1+u_3)\pi}{L_{DM}} + \frac{2\pi l}{L} + \frac{2\pi}{L_r}\right]\right|^{1/4} \\
&\left|\sin\left[\frac{(q-1)(u_2+u_4)\pi}{L_{DM}} + \frac{2\pi l}{L} + \frac{2\pi}{L_r}\right]\right|^{1/4}.
\end{aligned} \quad (28)$$

*Proof.* For the cases of $\tau = 1$ and $\tau = 2$, $\Lambda_p^{\tau=1}$ and $\Lambda_p^{\tau=2}$ may be obtained in the same way following the proof of Proposition 2. For the case of $\tau = 3$, we have $\mathbf{G}_r^2$ in (24), which implies that the activated layer is shifted twice away from the diagonal line. The corresponding determinant term in (25) may be evaluated by:

$$\begin{aligned}
\det(\mathbf{\Delta}) = &[4 - |1 + \phi_r^2 w_{L_DM}^{(q-1)(u_1+u_3)} w_L^{2l}|^2] \\
&[4 - |1 + \phi_r^2 w_{L_DM}^{(q-1)(u_2+u_4)} w_L^{2l}|^2],
\end{aligned} \quad (29)$$

which results in $\Lambda_p^{\tau=3}$ of (28). Moreover, for the case of $\tau = 4$, we have $\mathbf{G}_r^3 = (\mathbf{G}_r)^T$ in (24), which is equivalent to the case of using $\tau = 2$ associated with $\mathbf{G}_r$. □

Consequently, similar to DSTSK-DAST, the DSTSK-TAST's integer phase-rotation parameters $\{1 \le u_t \le L_{DM} - 1\}_{t=1}^{T}$ may also be obtained by brute-force exhaustive search for maximizing the diversity product of (25). However, unlike DSTSK-DAST, the ordering of $\{u_t\}_{t=1}^{T}$ may change $\Lambda_p$ for DSTSK-TAST due to the phase rotations of $\phi_r^{\tau-1}$. Nonetheless, the DSTSK-TAST's search space may still be reduced to $(\frac{L_{DM}}{2})^T$ number of combinations for candidate integers $\{u_t\}_{t=1}^{T}$, which are still supposed to be relatively prime to $L_{DM}$.

***Example 5:*** Let us now consider the DSTSK-TAST using $M = T = 2$ at the throughput of $R = \frac{\log_2 LTQ}{T} = 1.5$, where we have $L_{DM} = LQ = 4$. Since the DSTSK-TAST detection complexity order in Sec. IV-C is given by $\mathcal{O}(TQ)$, we start from the parameter combination of $Q = 1$, $L = 4$ and $L_r = \max\{LT, L_{DM}\} = 8$, and the exhaustive search gives $\mathbf{u} = [1,1]$ associated with $\Lambda_p = 0.5946$, which is the same as the diversity product of its DGC counterpart of Example 1 and that of its DSTSK-DAST counterpart of Example 3. Furthermore, once we further increase $Q$ and use the updated combination of $Q = 2$, $L = 2$ and $L_r = \max\{LT, L_{DM}\} = 4$, the exhaustive search gives $\mathbf{u} = [1,3]$ achieving $\Lambda_p = 0.7071$, which is higher than that of both DGC and DSTSK-DAST. The corresponding DSTSK-TAST signal matrices are summarized in Table VI. Specifically, compared to the DGC of Example 1, DSTSK-TAST achieves a higher $\Lambda_p = 0.7071$ at a lower detection complexity order of $\mathcal{O}(TQ = 4)$.

TABLE VI: Example of DSTSK-TAST($M = T = 2$) using $Q = 2$, $L = 2$, $L_{DM} = 4$, $L_r = 4$ and $\mathbf{u} = [1,3]$ at $R = 1.5$.

| Input bits | PSK symbol | Index $\tau$ | Index $q$ | Dispersion matrix | Data-carrying matrix |
|---|---|---|---|---|---|
| 000 | $x^0=1$ | $\tau=1$ | $q=1$ | $\mathbf{A}_{1,1} = \begin{bmatrix} 1 & 0 \\ 0 & 1 \end{bmatrix}$ | $\mathbf{X}=x^0\mathbf{A}_{1,1}=\begin{bmatrix} 1 & 0 \\ 0 & 1 \end{bmatrix}$ |
| 001 | $x^0=1$ | $\tau=1$ | $q=2$ | $\mathbf{A}_{1,2} = \begin{bmatrix} j & 0 \\ 0 & -j \end{bmatrix}$ | $\mathbf{X}=x^0\mathbf{A}_{1,2}=\begin{bmatrix} j & 0 \\ 0 & -j \end{bmatrix}$ |
| 010 | $x^0=1$ | $\tau=2$ | $q=1$ | $\mathbf{A}_{2,1} = \begin{bmatrix} 0 & j \\ j & 0 \end{bmatrix}$ | $\mathbf{X}=x^0\mathbf{A}_{2,1}=\begin{bmatrix} 0 & j \\ j & 0 \end{bmatrix}$ |
| 011 | $x^0=1$ | $\tau=2$ | $q=2$ | $\mathbf{A}_{2,2} = \begin{bmatrix} 0 & -1 \\ 1 & 0 \end{bmatrix}$ | $\mathbf{X}=x^0\mathbf{A}_{2,2}=\begin{bmatrix} 0 & -1 \\ 1 & 0 \end{bmatrix}$ |
| 100 | $x^1=-1$ | $\tau=1$ | $q=1$ | $\mathbf{A}_{1,1} = \begin{bmatrix} 1 & 0 \\ 0 & 1 \end{bmatrix}$ | $\mathbf{X}=x^1\mathbf{A}_{1,1}=\begin{bmatrix} -1 & 0 \\ 0 & -1 \end{bmatrix}$ |
| 101 | $x^1=-1$ | $\tau=1$ | $q=2$ | $\mathbf{A}_{1,2} = \begin{bmatrix} j & 0 \\ 0 & -j \end{bmatrix}$ | $\mathbf{X}=x^1\mathbf{A}_{1,2}=\begin{bmatrix} -j & 0 \\ 0 & j \end{bmatrix}$ |
| 110 | $x^1=-1$ | $\tau=2$ | $q=1$ | $\mathbf{A}_{2,1} = \begin{bmatrix} 0 & j \\ j & 0 \end{bmatrix}$ | $\mathbf{X}=x^1\mathbf{A}_{2,1}=\begin{bmatrix} 0 & -j \\ -j & 0 \end{bmatrix}$ |
| 111 | $x^1=-1$ | $\tau=2$ | $q=2$ | $\mathbf{A}_{2,2} = \begin{bmatrix} 0 & -1 \\ 1 & 0 \end{bmatrix}$ | $\mathbf{X}=x^1\mathbf{A}_{2,2}=\begin{bmatrix} 0 & 1 \\ -1 & 0 \end{bmatrix}$ |

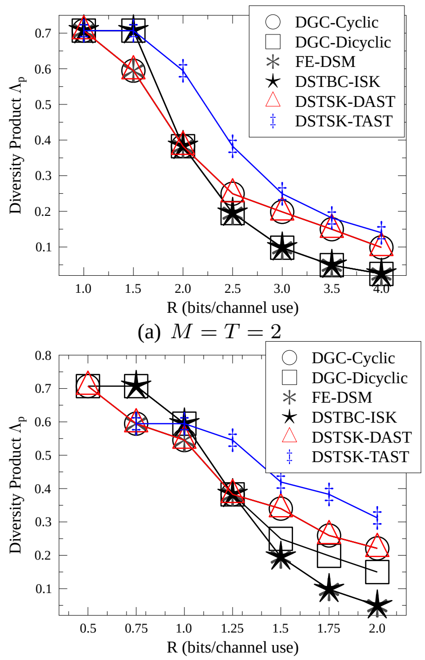


(a) $M = T = 2$

(b) $M = T = 4$

Fig. 5: Comparison of diversity products of finite-cardinality DSTM schemes.

***Example 6:*** For a DSTSK-TAST using $M = T = 4$ at $R = 1.25$, we obtain the parameters of $Q = 2$, $L = 4$, $L_{DM} = 8$, $L_r = 16$ and $\mathbf{u} = [1, 3, 7, 5]$, which achieves $\Lambda_p = 0.5453$ that is higher than $\Lambda_p = 0.3827$ of the DGC and DSTSK-DAST of Examples 2 and 4. The resultant DSTSK-TAST signal matrices are given by $\{\{\{\mathbf{X}^i = w_4^l \mathbf{A}_{\tau,q}\}_{l=0}^{3}\}_{\tau=1}^{4}\}_{q=1}^{2}$, where the dispersion matrix is given by $\mathbf{A}_{\tau,q} = w_{16}^{\tau-1}\text{diag}([w_8^{(q-1)}, w_8^{3(q-1)}, w_8^{7(q-1)}, w_8^{5(q-1)}])\mathbf{G}_r^{\tau-1}$. The associated detection complexity order is $\mathcal{O}(TQ = 8)$, which is lower than the DGC's $\mathcal{O}(I = 32)$ in Example 2.

### *E. Comparison of Diversity Products*

All of the diversity-oriented finite-cardinality DSTM schemes are summarized in Table VII, which may be categorized into three types. The first type is the classic cyclic and dicyclic DGCs, which actively maximize their diversity products by using the parameters $\mathbf{u} = [u_1, \cdots, u_T]$, but the DGC detection complexity grows exponentially with the throughput, as demonstrated by Table VII. The second type is the full-diversity FE-DSM and DSTBC-ISK schemes that achieve a non-zero $\Lambda_p$ in Table VII. However, in the absence of diversity gain maximization, both FE-DSM and DSTBC-ISK generally suffer from a performance loss compared to the DGCs as the throughput increases. Nonetheless, as a benefit, both FE-DSM and DSTBC-ISK are capable of invoking the single-stream ML detection. Finally, the third type is constituted by our proposed DSTSK-DAST and DSTSK-TAST featured in Table VII, which are capable of achieving a actively maximized diversity gain at the low-cost of a single-stream ML detection complexity.

The diversity products of (5a) achieved by the above DSTM schemes are compared in Fig. 5, where the parameters are summarized in Table VIII. Firstly, Fig. 5 evidences that DSTSK-ISK achieves higher diversity products than FE-DSM at $R = 1.5$ for $M = T = 2$ and $R = \{0.75, 1.0\}$ for $M = T = 4$, but the diversity products of both DSTSK-ISK and FE-DSM decrease rapidly and become substantially lower than that of DGC-cyclic as the throughput increases. Secondly, it is evidenced by Fig. 5 that the proposed DSTSK-DAST is capable of achieving exactly the same diversity gains as DGC-cyclic, while the proposed DSTSK-TAST is capable of achieving even further improved diversity gains, apart from the low-throughput exceptions of $R = 1$ for $M = T = 2$ and $R = 0.75$ for $M = T = 4$, where the diversity products of DSTSK-TAST, DSTSK-DAST and DGC-cyclic are the same. Once again, the diversity advantages of DSTSK-DAST and DSTSK-TAST are achieved at a substantially lower detection complexity than that of DGC. Moreover, we also note that the better-performing DSTSK-TAST has a higher detection complexity order of $\mathcal{O}(QT)$ than $\mathcal{O}(Q)$ of DSTSK-DAST, despite the fact that neither of the two single-stream ML detection complexities increase with the constellation size. Our more detailed performance versus complexity comparisons will be presented in Sec. VI.

## V. Amplitude-Phase Shift Keying (APSK) and Diversity-Rate (DR) Tradeoff

In order to improve the throughput, in Sec. V-A, we further extend the SE-APSK design of [40] to the ME-APSK, while a generic DR arrangement is conceived for a practical DSTM diversity-throughput tradeoff design in Sec. V-B.

### *A. Multi-Element (ME) Amplitude-Phase Shift Keying (APSK)*

According to [40], the generic $L_A$-level ring-amplitude is applied to the PSK signals in (1) by the Differential Amplitude Shift Keying (DASK) as $\Gamma_n = \gamma_{n-1}\Gamma_{n-1}$, where $\{\Gamma_{n-1} = \frac{\alpha^{\mu_{n-1}}}{\sqrt{\beta}}, \Gamma_n = \frac{\alpha^{\mu_n}}{\sqrt{\beta}}\}$ and $\{\gamma_{n-1} = \alpha^a\}_{a=0}^{L_A-1}$ represent the transmitted ring-amplitudes and data-carrying ring-amplitude, respectively, while $\alpha$ and $\beta = \frac{\sum_{\mu=0}^{L_A-1}\alpha^{2\mu}}{L_A}$ respectively represent the ring ratio and the associated normalization factor. More explicitly, the indices of the transmitted ring-amplitudes $\{\Gamma_{n-1}, \Gamma_n\}$ are given by the integers $\{\mu_{n-1}, \mu_n\} \in [0, L_A - 1]$, while the data-carrying ring-amplitude modulates the difference between $\mu_{n-1}$ and $\mu_n$ as $a = [(\mu_{n-1} + \check{a}) \textbf{ mod } L_A] - \mu_{n-1}$, where $a$ is the Gray coded version of the natural index $\check{a}$.

In order to further extend the SE design of [40] and the two/four-ring ME design of [33], [34], the differential encoding of (1) may be revised for the generic ME-APSK as [33], [34]:

$$\widetilde{\mathbf{S}}_n = \mathbf{X}_{n-1}\widetilde{\mathbf{S}}_{n-1}\mathbf{\Lambda}_{n-1}, \tag{30}$$

where the $(T \times T)$-element data-carrying ring-amplitude matrix is $\mathbf{\Lambda}_{n-1} = \text{diag}([\gamma_{n-1,1}, \cdots, \gamma_{n-1,T}])$, which forms a star-QAM constellation for $\widetilde{\mathbf{S}}_{n-1} = \mathbf{S}_{n-1}\text{diag}([\Gamma_{n-1,1}, \cdots, \Gamma_{n-1,T}])$ and $\widetilde{\mathbf{S}}_n = \mathbf{S}_n\text{diag}([\Gamma_{n,1}, \cdots, \Gamma_{n,T}])$ owing to the DASK of $\{\Gamma_{n,t} = \gamma_{n-1,t}\Gamma_{n-1,t}\}_{t=1}^{T}$.

It was proven in [34] that for a single-RF sparse signal matrix $\widetilde{\mathbf{S}}_{n-1}$, we have the relationship of $\widetilde{\mathbf{S}}_{n-1}\mathbf{\Lambda}_{n-1} = \overline{\mathbf{\Lambda}}_{n-1}\widetilde{\mathbf{S}}_{n-1}$, where the permuted matrix is given by $\overline{\mathbf{\Lambda}}_{n-1} =$

TABLE VII: Summary of diversity-oriented finite-cardinality DSTM schemes.

| **DSTM scheme** | **Diversity product** | **Throughput** | **Detection complexity** |
|---|---|---|---|
| DGC-cyclic | $\Lambda_p = \min_{\forall l\neq 0} \prod_{t=1}^{T} \left|\sin\left(\frac{\pi}{L}u_t l\right)\right|^{1/T}$ | $R = \frac{\log_2 L}{T}$ | $\mathcal{O}(L = 2^{RT})$ |
| DGC-dicyclic | $\Lambda_p = \min\{\frac{1}{\sqrt{2}}, \min_{\forall l\neq 0} \prod_{t=1}^{T/2} \left|\sin\left(\frac{\pi}{L}u_t l\right)\right|^{2/T}\}$ | $R = \frac{\log_2 2L}{T}$ | $\mathcal{O}(2L = 2^{RT})$ |
| FE-DSM | $\Lambda_p = \min_{\forall (l\neq 0 \vert\vert q\neq 1)} \prod_{t=1}^{T} \left|\sin\left[\frac{\pi}{L}l + \frac{\pi(Lt-L+1)}{LT}(q-1)\right]\right|$ | $R = \frac{\log_2 L + \log_2 T}{T}$ | $\mathcal{O}(T)$ |
| DSTBC-ISK | $T=2$: $\Lambda_p = \min\{\sin(\pi/L), \frac{1}{\sqrt{2}}\}$ <br> $T \geq 4$: $\Lambda_p = \min\{\sin(\pi/L), \frac{1}{\sqrt{2}}\sqrt{\sin(\frac{4\pi}{QL})}\}$ | $R = \frac{\log_2 L + \log_2 T}{T}$ | $\mathcal{O}(T)$ |
| DSTSK-DAST | $\Lambda_p = \min_{\forall (l\neq 0 \vert\vert q\neq 1)} \prod_{t=1}^{T} \left|\sin\left[\frac{\pi(qu_t - u_t + lL_{DM}/L)}{L_{DM}}\right]\right|^{1/T}$ | $R = \frac{\log_2 L + \log_2 Q}{T}$ | $\mathcal{O}(Q)$ |
| DSTSK-TAST | $\Lambda_p = \frac{1}{2}\min_{\forall i\neq 0}\ \det\left[(\mathbf{I}_T - x^l\mathbf{A}_{\tau,q})^H(\mathbf{I}_T - x^l\mathbf{A}_{\tau,q})\right]^{\frac{1}{2T}}$ <br> where $\mathbf{A}_{\tau,q} = \phi_r^{\tau-1}\text{diag}([w_{L_{DM}}^{(q-1)u_1}, \cdots, w_{L_{DM}}^{(q-1)u_T}])\mathbf{G}_r^{\tau-1}$ | $R = \frac{\log_2 L + \log_2 Q + \log_2 T}{T}$ | $\mathcal{O}(QT)$ |

TABLE VIII: Parameters of DSTSK-TAST, DSTSK-DAST and DGC-cyclic used for Fig. 5.

(a) DSTSK-TAST, $M = T = 2$

| | |
|---|---|
| $R = 1.0$: $Q = 1$, $L = 2$, $L_{DM} = 2$, $L_r = 4$, $u = [1, 1]$ | $R = 1.5$: $Q = 2$, $L = 2$, $L_{DM} = 4$, $L_r = 4$, $u = [1, 3]$ |
| $R = 2.0$: $Q = 4$, $L = 2$, $L_{DM} = 8$, $L_r = 8$, $u = [1, 3]$ | $R = 2.5$: $Q = 2$, $L = 8$, $L_{DM} = 16$, $L_r = 16$, $u = [3, 13]$ |
| $R = 3.0$: $Q = 4$, $L = 8$, $L_{DM} = 32$, $L_r = 32$, $u = [29, 3]$ | $R = 3.5$: $Q = 4$, $L = 16$, $L_{DM} = 64$, $L_r = 64$, $u = [7, 57]$ |
| $R = 4.0$: $Q = 8$, $L = 16$, $L_{DM} = 128$, $L_r = 128$, $u = [3, 117]$ | |

(b) DSTSK-DAST, $M = T = 2$

| | |
|---|---|
| $R = 1.0$: $Q = 1$, $L = 4$, $L_{DM} = 4$, $u = [1, 1]$ | $R = 1.5$: $Q = 2$, $L = 4$, $L_{DM} = 8$, $u = [1, 5]$ |
| $R = 2.0$: $Q = 2$, $L = 8$, $L_{DM} = 16$, $u = [1, 9]$ | $R = 2.5$: $Q = 4$, $L = 8$, $L_{DM} = 32$, $u = [1, 25]$ |
| $R = 3.0$: $Q = 16$, $L = 4$, $L_{DM} = 64$, $u = [1, 37]$ | $R = 3.5$: $Q = 8$, $L = 16$, $L_{DM} = 128$, $u = [1, 81]$ |
| $R = 4.0$: $Q = 64$, $L = 4$, $L_{DM} = 256$, $u = [75, 255]$ | |

(c) DGC-cyclic, $M = T = 2$

| | | | |
|---|---|---|---|
| $R = 1.0$: $L = 4$, $u = [1, 1]$ | $R = 1.5$: $L = 8$, $u = [1, 3]$ | $R = 2.0$: $L = 16$, $u = [1, 7]$ | $R = 2.5$: $L = 32$, $u = [1, 7]$ |
| $R = 3.0$: $L = 64$, $u = [1, 19]$ | $R = 3.5$: $L = 128$, $u = [1, 47]$ | $R = 4.0$: $L = 256$, $u = [1, 75]$ | |

(d) DSTSK-TAST, $M = T = 4$

| | |
|---|---|
| $R{=}0.75$: $Q{=}1$, $L{=}2$, $L_{DM}{=}2$, $L_r{=}8$, $u{=}[1, 1, 1, 1]$ | $R{=}1.0$: $Q{=}2$, $L{=}2$, $L_{DM}{=}4$, $L_r{=}8$, $u{=}[1, 1, 3, 3]$ |
| $R{=}1.25$: $Q{=}2$, $L{=}4$, $L_{DM}{=}8$, $L_r{=}16$, $u{=}[1, 3, 7, 5]$ | $R{=}1.5$: $Q{=}4$, $L{=}4$, $L_{DM}{=}16$, $L_r{=}32$, $u{=}[1, 5, 15, 7]$ |
| $R{=}1.75$: $Q{=}4$, $L{=}8$, $L_{DM}{=}32$, $L_r{=}32$, $u{=}[5, 25, 11, 31]$ | $R{=}2.0$: $Q{=}8$, $L{=}8$, $L_{DM}{=}64$, $L_r{=}64$, $u{=}[15, 41, 57, 63]$ |

(e) DSTSK-DAST, $M = T = 4$

| | |
|---|---|
| $R = 0.5$: $Q = 1$, $L = 4$, $L_{DM} = 4$, $u = [1, 1, 1, 1]$ | $R = 0.75$: $Q = 2$, $L = 4$, $L_{DM} = 8$, $u = [1, 1, 5, 5]$ |
| $R = 1.0$: $Q = 4$, $L = 4$, $L_{DM} = 16$, $u = [1, 5, 9, 13]$ | $R = 1.25$: $Q = 4$, $L = 8$, $L_{DM} = 32$, $u = [7, 15, 23, 31]$ |
| $R = 1.5$: $Q = 16$, $L = 4$, $L_{DM} = 64$, $u = [1, 29, 37, 49]$ | $R = 1.75$: $Q = 32$, $L = 4$, $L_{DM} = 128$, $u = [83, 91, 103, 127]$ |
| $R = 2.0$: $Q = 64$, $L = 4$, $L_{DM} = 256$, $u = [1, 41, 137, 221]$ | |

(f) DGC-cyclic, $M = T = 4$

| | | |
|---|---|---|
| $R = 0.5$: $L = 4$, $u = [1, 1, 1, 1]$ | $R = 0.75$: $L = 8$, $u = [1, 1, 3, 3]$ | $R = 1.0$: $L = 16$, $u = [1, 3, 5, 7]$ |
| $R = 1.25$: $L = 32$, $u = [1, 7, 9, 15]$ | $R = 1.5$: $L = 64$, $u = [1, 15, 27, 29]$ | $R = 1.75$: $L = 128$, $u = [1, 25, 37, 45]$ |
| $R = 2.0$: $L = 256$, $u = [1, 35, 41, 119]$ | | |

$\text{diag}([\gamma_{n-1,t_1}, \cdots, \gamma_{n-1,t_T}])$, as $\{t_\iota\}_{\iota=1}^{T}$ denotes the activation index of $\iota$-th row in $\widetilde{\mathbf{S}}_{n-1}$. As a result, the received signal model of (2) may be further extended as $\mathbf{Y}_n = \mathbf{X}_{n-1}\overline{\mathbf{\Lambda}}_{n-1}(\mathbf{Y}_{n-1} - \mathbf{V}_{n-1}) + \mathbf{V}_n$ under the assumption of $\mathbf{H}_{n-1} = \mathbf{H}_n$, which leads to the following ME-APSK detection:

$$\{\hat{\mathbf{X}}_{n-1}, \hat{\overline{\mathbf{\Lambda}}}_{n-1}\} = \arg\min_{\substack{\forall \mathbf{X}_{n-1} \in \{\mathbf{X}^i\}_{i=0}^{I} \\ \forall \overline{\mathbf{\Lambda}}_{n-1} \in \{\overline{\mathbf{\Lambda}}^{a_1,\cdots,a_T}\}_{a_1,\cdots,a_T \in [0, L_A - 1]}}} \left\|\mathbf{Y}_n - \mathbf{X}_{n-1}\overline{\mathbf{\Lambda}}_{n-1}\mathbf{Y}_{n-1}\right\|^2. \tag{31}$$

The ME-DASK design of (30) improves the DSTM throughput from $R{=}\frac{\log_2 I}{T}$ to $R{=}\frac{\log_2 I + T\log_2 L_A}{T}$, but the detection complexity of (31) also grows exponentially with the throughput as $\mathcal{O}(IL_A^T)$.

Against this background, we further propose to invoke the single-stream ML detection for our ME-APSK applications. More explicitly, the decision metric of (31) may be further extended as:

$$\begin{aligned}\left\|\mathbf{Y}_n - \mathbf{X}_{n-1}\overline{\mathbf{\Lambda}}_{n-1}\mathbf{Y}_{n-1}\right\|^2 &= \kappa_n^2 + \textstyle\sum_{\iota=1}^{T} \gamma_{n-1,t_\iota}^2 \|\mathbf{Y}_{n-1}^{\iota}\|^2 \\ &\quad - 2\Re\left[\text{tr}(\overline{\mathbf{\Lambda}}_{n-1}\mathbf{X}_{n-1}^H\mathbf{Z})\right] \\ &= \kappa_n^2 + \textstyle\sum_{\iota=1}^{T} \kappa_{n-1,\iota}^2(\gamma_{n-1,t_\iota} - \overline{z}_{\iota,\iota}/\kappa_{n-1,\iota}^2)^2 - \sum_{\iota=1}^{T}\overline{z}_{\iota,\iota}^2/\kappa_{n-1,\iota}^2,\end{aligned} \tag{32}$$

where we define $\kappa_n^2 = \|\mathbf{Y}_n\|^2$ and $\mathbf{Z} = \mathbf{Y}_n\mathbf{Y}_{n-1}^H$, while $\mathbf{Y}_{n-1}^{\iota}$ denotes the $\iota$-th row in $\mathbf{Y}_{n-1}$. We also define $\kappa_{n-1,\iota}^2 = \|\mathbf{Y}_{n-1}^{\iota}\|^2$, and $\overline{z}_{\iota,\iota}$ denotes the element on the $\iota$-th row and $\iota$-th column of $\overline{\mathbf{Z}} = \Re(\mathbf{X}^H\mathbf{Z})$. Owing to the fact that $(\kappa_n^2 - \sum_{\iota=1}^{T}\overline{z}_{\iota,\iota}^2/\kappa_{n-1,\iota}^2)$ in (32) is a constant for the ring-amplitudes, the ME-APSK detection may be decoupled as $\{\gamma_{n-1,t_\iota} = \mathbb{M}_{\text{DASK}}^{-1}(\overline{z}_{\iota,\iota}/\kappa_{n-1,\iota}^2)\}_{\iota=1}^{T}$ without any performance loss, where the linearized DASK detector is given by (48) of [40]. As a result, when the ME-APSK design is applied to the finite-cardinality schemes of DSM, DSTBC-ISK, FE-DSM, DSTSK-DAST and DSTSK-TAST, both the linearized PSK detector $\mathbb{M}_{\text{PSK}}^{-1}(\cdot)$ exemplied in (15) and the DASK detector $\mathbb{M}_{\text{DASK}}^{-1}(\cdot)$ are invoked, so that the resultant single-stream ML detection complexity does not grow with the star QAM constellation size.

TABLE IX: Summary of detection complexity of DSM using ME-APSK.

| Scheme | Complexity order | Real-valued multiplications |
|---|---|---|
| Two-ring-amplitude design [33] | $\mathcal{O}(IL_A^T)$ | $(6T^2N + 8T^2N)IL_A^T$ |
| Four-ring-amplitude design [34] | $\mathcal{O}(IL_A^T)$ | $(6T^2N + 2T^2N)IL_A^T$ |
| New generic design | $\mathcal{O}(\overline{M})$ | $4T^2N + (1 + 6T^2N + 6T^3)\overline{M}$ |

Let us consider the DSM example of Sec. (II-D) using ME-ASK. Firstly, in order to detect the unitary matrix $\mathbf{X}$ in (32), according to Sec. IV of [40], the PSK detector is invoked $\overline{M}T$ times as $\{\{\hat{l}_{\overline{m},t} = \mathbb{M}_{\text{PSK}}^{-1}((\mathbf{Z}(t, \mathrm{a}_{\overline{m},t}))\}_{\overline{m}=1}^{\overline{M}}\}_{t=1}^{T}$, where $\mathbf{Z}(t, \mathrm{a}_{\overline{m},t})$ denotes the element on the $t$-th row and

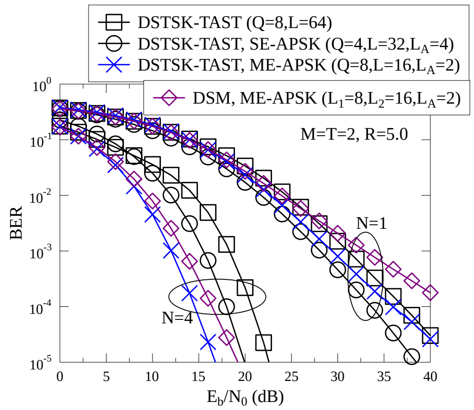


Fig. 6: Performance of DSTSK-TAST employing ME-APSK, where we have $M = T = 2$ and $R = 5.0$.

$a_{\bar{m},t}$-column in $\mathbf{Z} = \mathbf{Y}_n\mathbf{Y}_{n-1}^H$. Following this, a total of $\overline{M}$ legitimate candidates can be formed for $\mathbf{X}$ in (32) according to $\{\{\hat{l}_{\overline{m},t}\}_{\overline{m}=1}^{\overline{M}}\}_{t=1}^T$. Secondly, the DASK detector is invoked $\overline{M}T$ times as $\{\{\hat{a}_{\overline{m},\iota} = \mathbb{M}_{\text{DASK}}^{-1}(\overline{z}_{\iota,\iota}/\kappa_{n-1,\iota}^2)\}_{\overline{m}=1}^{\overline{M}}\}_{\iota=1}^T$, which further forms $\overline{M}$ candidates for $\mathbf{\Lambda}_{n-1}$ in (32). As a result, the permutation index can be obtained by evluating (32) for a reduced number of $\overline{M}$ times as $\hat{\overline{m}} = \arg\min_{\overline{m}\in[1,\overline{M}]} \left\|\mathbf{Y}_n - \mathbf{X}_{n-1}\overline{\mathbf{\Lambda}}_{n-1}\mathbf{Y}_{n-1}\right\|^2$. Finally, the $T$ data-carrying PSK and ring-amplitude indices are given by $\{\hat{l}_t = \hat{l}_{\hat{\overline{m}},t}\}_{t=1}^T$ and $\{\hat{a}_t = \hat{a}_{\hat{\overline{m}},t}\}_{t=1}^T$, respectively. In summary, the complexity comparison between the proposed generic design and the existing ME-APSK solutions [33], [34] is shown in Table IX.

It is straightforward to see that $\overline{\mathbf{\Lambda}}_{n-1}$ of (32) does not comply with the full-rank requirement of (4), as a pair of $\overline{\mathbf{\Lambda}}_{n-1}$ and $\overline{\mathbf{\Lambda}}'_{n-1}$ associated with $\gamma_{n-1,t_1} = \gamma'_{n-1,t_1}$ and $\{\gamma_{n-1,t_\iota} \neq \gamma'_{n-1,t_\iota}\}_{\iota=2}^T$ has rank-1. It is exemplied by Fig. 6 that for the case of DSTSK-TAST using $N = 1$, the full-diversity SE-APSK arrangement performs better. However, Fig. 6 also demonstrates that for the case of using $N = 4$, the ME-APSK arrangement helps the DSTSK-TAST scheme once again to achieve a performance advantage over DSM.

Moreover, as a DASK counterpart, the ASK using the absolute-amplitude of $\Gamma_n = \gamma_{n-1} = \frac{\alpha^{\bar{a}}}{\sqrt{\beta}}$ is capable of achieving a better performance in channel coded scenarios [40], but this is beyond the scope of this treatise. Nonetheless, for the sake of technical completeness, we note that for the applications of ME-APSK design using ASK, the DASK's $\{\gamma_{n-1,t}\}_{t=1}^T$ in $\mathbf{\Lambda}_{n-1}$ values of (30) are replaced by $\{\gamma_{n-1,t}/\Gamma_{n-1,t}\}_{t=1}^T$, while the single-stream ASK detector is invoked as $\{\gamma_{n-1,t_\iota} = \mathbb{M}_{\text{ASK}}^{-1}(\Gamma_{n-1,t_\iota}\overline{z}_{\iota,\iota}/\kappa_{n-1,\iota}^2)\}_{\iota=1}^T$ for (32) according to (49) in [40].

### *B. Diversity-Rate Tradeoff*

The DR arrangement in [37], [38] partitions the $(T \times T)$ DSTM signal space into $(T_D \times T_D)$ sub-blocks, where $V = T/T_D$ number of $(T_D \times T_D)$ DSTM sub-blocks are transmitted in a permuted manner. This is exemplied in Fig. 7 for the case of using $M = T = 4$ and $V = 2$, where two $2 \times 2$ DSTM sub-blocks are permuted in the $4 \times 4$ DSTM signal space. As a result, the DR design retains a reduced diversity order of $T_D$ in exchange for an improved throughput of $R = \frac{\sum_{u=1}^V \log_2 I_u + \log_2 V}{T}$, where $\{I_u\}_{u=1}^V$ denotes the cardinality of the $u$-th constituent DSTM scheme, while the permutation index $\{v\}_{v=1}^V$ carries an extra number of $\log_2 V$ bits. Furthermore, since there is no interference between the DSTM sub-blocks, the single-stream ML detection may be also invoked. Explicitly, the DR design forms the $(T \times T)$-element signal matrix as:

$$\mathbf{X}^i = \left(\mathbf{G}_r^{v-1} \otimes \mathbf{I}_{T_D}\right) \text{diag}\{\overline{\mathbf{X}}_1^{i_1}, \cdots, \overline{\mathbf{X}}_V^{i_V}\}, \tag{33}$$

where instead of using a FE matrix in [37], [38], the $(V \times V)$-element switching matrix $\mathbf{G}_r$ defined in (22) is invoked for the generic DSTM design. Moreover, the $(T_D \times T_D)$-element signal matrix $\{\overline{\mathbf{X}}_u^{i_u}\}_{u=1}^V$ of (33) denotes the constituent DSTM sub-block.

As a result, upon obtaining the received signals of (2), the decision metric of (3) may be further extended for the DR detection as:

$$\left\|\mathbf{Y}_n - \mathbf{X}^i\mathbf{Y}_{n-1}\right\|^2 = \kappa_n^2 + \sum_{u=1}^V \left\{\left\|\mathbf{Y}_{n-1,(u)}\right\|^2 - 2\Re\left[\text{tr}\left((\overline{\mathbf{X}}_u^{i_u})^H \overline{\mathbf{Z}}_{(u)}^v\right)\right]\right\}, \tag{34}$$

where we define the $(T_D \times N)$-element matrix $\mathbf{Y}_{n-1,(u)} = Y_{n-1}([(u-1)T_D + 1 : uT_D, :])$ as the submatrix taken from the $[(u-1)T_D + 1]$-th to the $(uT_D)$-th rows of $Y_{n-1}$, and we also define the $(T_D \times T_D)$-element matrix $\overline{\mathbf{Z}}_{(u)}^v = \overline{\mathbf{Z}}^v([(u-1)T_D + 1 : uT_D, (u-1)T_D + 1 : uT_D])$ as the submatrix taken from the $[(u-1)T_D+1]$-th to the $(uT_D)$-th rows and columns of $\overline{\mathbf{Z}}^v = \left(\mathbf{G}_r^{v-1} \otimes \mathbf{I}_{T_D}\right)^H \mathbf{Y}_n\mathbf{Y}_{n-1}^H$. Moreover, we note that $\sum_{u=1}^V \left\|\mathbf{Y}_{n-1,(u)}\right\|^2 = \kappa_{n-1}^2$ in (34) is a constant. As a result, the detection of $\{\overline{\mathbf{X}}_u^{i_u}\}_{u=1}^V$ is decoupled in Eq. (34), which is detailed in the pseudocode of Table X. Moreover, when the constituent DSTM sub-blocks use FE-DSM, DSTBC-ISK as well as the proposed DSTSK-DAST and DSTSK-TAST schemes, their respective single-stream ML detector may be directly invoked for line 4 in Table X.

In order to once again introduce star-QAM signalling without compromising the diversity, we further propose the DR-APSK design, where a single ring-amplitude is assigned to each $(T_D \times T_D)$-element DSTM sub-

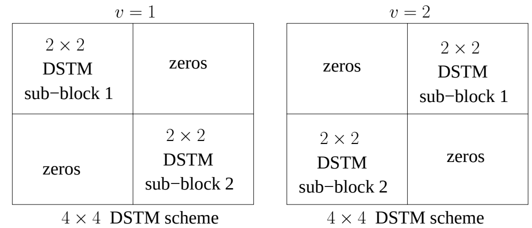


Fig. 7: Examples of a $(4 \times 4)$ DSTM scheme using DR associated with $M = T = 4$ and $V = 2$.

TABLE X: Pseudocode for the single-stream ML detection of DSTM-DR.

1: **for** $v = 1$ **to** $V$
2: $\quad \overline{\mathbf{Z}}^v = \left(\mathbf{G}_r^{v-1} \otimes \mathbf{I}_{T_D}\right)^H \mathbf{Y}_n\mathbf{Y}_{n-1}^H$
3: $\quad$ **for** $u = 1$ **to** $V$
4: $\quad\quad \hat{i}_{v,u} = \arg\max_{\forall i_{v,u}\in[0,I_u-1]} \Re\left[\text{tr}\left((\overline{\mathbf{X}}_u^{i_{v,u}})^H \overline{\mathbf{Z}}_{(u)}^v\right)\right]$
5: $\quad\quad d_{v,u} = \Re\left[\text{tr}\left((\overline{\mathbf{X}}_u^{\hat{i}_{v,u}})^H \overline{\mathbf{Z}}_{(u)}^v\right)\right]$
6: $\quad$ **end for**
7: **end for**
8: $\hat{v} = \max_{\forall v\in\{0,V-1\}} \sum_{u=1}^V d_{v,u}$
9: $\{\hat{i}_u = \hat{i}_{\hat{v},u}\}_{u=1}^V$

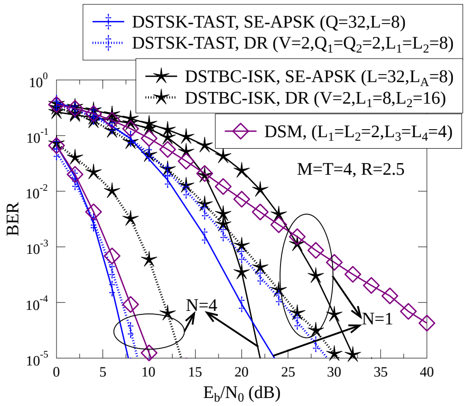


(a) $M=T=4$, $R=2.5$

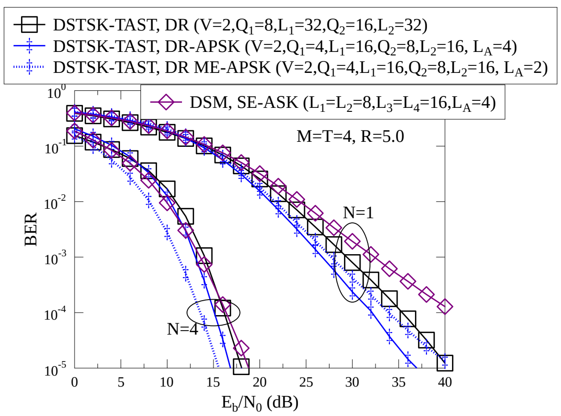


(b) $M=T=4$, $R=5.0$

Fig. 8: Performance of DSTSK-TAST and DSTBC-ISK employing the DR and APSK arrangements, where we have $M=T=4$.

block. More explicitly, for the DR-APSK design, the $(T\times T)$-element ring-amplitude matrix in (30) is given by $\mathbf{\Lambda}_{n-1}=\text{diag}([\gamma_{n-1,1}\mathbf{I}_{T_D},\cdots,\gamma_{n-1,V}\mathbf{I}_{T_D}])$. The resultant star QAM signal matrices are $\widetilde{\mathbf{S}}_{n-1}=\mathbf{S}_{n-1}\text{diag}([\Gamma_{n-1,1}\mathbf{I}_{T_D},\cdots,\Gamma_{n-1,V}\mathbf{I}_{T_D}])$ and $\widetilde{\mathbf{S}}_{n}=\mathbf{S}_{n}\text{diag}([\Gamma_{n,1}\mathbf{I}_{T_D},\cdots,\Gamma_{n,V}\mathbf{I}_{T_D}])$, where we have $\{\Gamma_{n,u}=\gamma_{n-1,u}\Gamma_{n-1,u}\}_{u=1}^{V}$ for using DASK. The sparse matrix feature leads to the relationship of $\widetilde{\mathbf{S}}_{n-1}\mathbf{\Lambda}_{n-1}=\overline{\mathbf{\Lambda}}_{n-1}\widetilde{\mathbf{S}}_{n-1}$, where the permuted matrix is $\overline{\mathbf{\Lambda}}_{n-1}=\text{diag}([\gamma_{n-1,t_1}\mathbf{I}_{T_D},\cdots,\gamma_{n-1,t_V}\mathbf{I}_{T_D}])$, as $\{t_\iota\}_{\iota=1}^{V}$ denotes the sub-block activation index. As a result, the decision metric of (34) is revised for DR-APSK as:

$$\begin{aligned}\left\|\mathbf{Y}_n-\mathbf{X}^i\overline{\mathbf{\Lambda}}^{a_1,\cdots,a_V}\mathbf{Y}_{n-1}\right\|^2&=\kappa_n^2\\+\sum_{u=1}^{V}\Big\{\gamma_{n-1,t_u}^2\left\|\mathbf{Y}_{n-1,(u)}\right\|^2&-2\gamma_{n-1,t_u}\Re\Big[\text{tr}\Big((\overline{\mathbf{X}}_u^{i_u})^H\overline{\mathbf{Z}}_{(u)}^{v}\Big)\Big]\Big\}.\end{aligned}\tag{35}$$

Hence, following the unitary matrix detection of line 4 in Table X, the ring-amplitude detection is also decoupled as $\{\gamma_{n-1,t_\iota}=\mathbb{M}_{\text{DASK}}^{-1}(\Re\left[\text{tr}\left((\overline{\mathbf{X}}_u^{\hat{i}_{v,u}})^H\overline{\mathbf{Z}}_{(u)}^{v}\right)\right]/\left\|\mathbf{Y}_{n-1,(u)}\right\|^2)\}_{\iota=1}^{V}$, which leads to the ring-amplitude indices $\hat{a}_{v,u}$. Accordingly, the decision metric of line 5 in Table X may be revised for DR-APSK as $d_{v,u}=(\gamma^{\hat{a}_{v,u}})^2\left\|\mathbf{Y}_{n-1,(u)}\right\|^2-2\gamma^{\hat{a}_{v,u}}\Re\left[\text{tr}\left((\overline{\mathbf{X}}_u^{\hat{i}_{v,u}})^H\overline{\mathbf{Z}}_{(u)}^{v}\right)\right]$. Finally, the detected ring-amplitude indices are given by $\{\hat{a}_u=\hat{a}_{\hat{v},u}\}_{u=1}^{V}$ after line 9 in Table X.

Moreover, the DR design may also invoke the SE-APSK of [40] and the ME-APSK of Sec. V-A. More explicitly, Fig. 8(a) exemplifies that for the case of $M=T=4$ and $R=2.5$, DSTBC-ISK using DR substantially improves the performance of DSTBC-ISK using SE-APSK, but the DR design does not appear to be beneficial for DSTSK-TAST. This is because DSTSK-TAST actively maximizes its rank-4 diversity gain for $M=T=4$, which is more advantageous than its DR applications. Nonetheless, for the example of using $M=T=4$ at a very high rate of $R=5.0$ that conveys a total of 20 bits, optimizing the diversity gain for the DSTSK-TAST cardinality of $2^{20}$ becomes unrealistic. Against this background, the DSTSK-TAST using DR may invoke a pair of constituent DSTSK-TAST schemes of $(Q_1,L_1)=(8,32)$ and $(Q_1,L_1)=(16,32)$ that are optimized for $M=T=2$ at $R=4.5$ and $R=5.0$, respectively. As a result, it is confirmed in Fig. 8(b) that for the case of $M=T=4$ and $R=5.0$, the DSTSK-TAST using DR-ASK achieves the best performance for $N=1$, while the DSTSK-TAST using DR and ME-ASK ensures a further diversity gain over DSM for $N=4$.

## VI. Performance Results

First of all, in Sec. VI-A, the performance results of the full-diversity design are presented, where $M=\{2,4\}$ TAs and a small number of $N=\{1,2\}$ RAs are used. Secondly, the diversity-throughput tradeoff is further discussed in Sec. VI-B using both small and large number of $N=\{1,2,4,8,16\}$ RAs.

### A. Performance Results of Full-Diversity Design

The parameters of DSTSK-TAST, DSTSK-DAST and DGC-cyclic at high throughputs used in this section are summarized in Table XI, where the parameters of the low-throughput arrangements are the ones given in Table VIII. The parameters for DSTBC-ISK, FE-DSM and DSM can be retrieved from [31], [32], [38], [40]. Moreover, the star-QAM ring-amplitude ratios of $\alpha=\{2.0,1.4,1.2,1.1\}$ are used for $L_A=\{2,4,8,16\}$, respectively.

The performance comparisons are portrayed both in terms of their DCMC capacity and their BER performance in Fig. 9 for the case of $M=T=2$ and $R=2.0$. The evaluation of DSTM's DCMC capacity can be found in [40]. Fig. 9 demonstrates that the proposed DSTSK-DAST exhibits a similar performance to the classic DGC-cyclic, where both DSTSK-DAST and DGC-cyclic achieve substantial diversity gains over DSM. Furthermore, it is also evidenced by Fig. 9 that the new DSTSK-TAST achieves an even further improved performance over DGC-cyclic. We once again note that the diversity advantages of DSTSK-DAST and DSTSK-TAST are achieved at a substantially lower detection complexity than DGC-cyclic.

The performance results of the finite-cardinality DSTM schemes and their SISO counterparts of DPSK/ADPSK are summarized in terms of the $E_b/N_0$ required for achieving BER=$10^{-4}$ in Fig. 10 for the case of $M=T=\{2,4\}$ and $N=1$, while the corresponding complexity comparisons are portayed in Fig. 11. The complexities are evaluated in terms of the total number of real-valued multiplications, which are

TABLE XI: Parameters of DSTSK-TAST, DSTSK-DAST and DGC-cyclic used used in Sec. VI-A.

(a) DSTSK-TAST, SE-APSK, $M = T = 2$

| | |
|---|---|
| $R{=}3.0$: $Q{=}2$, $L{=}8$, $L_{DM}{=}16$, $L_r{=}16$, $u{=}[3, 13]$, $L_A{=}2$ | $R{=}3.5$: $Q{=}4$, $L{=}8$, $L_{DM}{=}32$, $L_r{=}32$, $u{=}[29, 3]$, $L_A{=}2$ |
| $R{=}4.0$: $Q{=}4$, $L{=}8$, $L_{DM}{=}32$, $L_r{=}32$, $u{=}[29, 3]$, $L_A{=}4$ | $R{=}4.5$: $Q{=}4$, $L{=}16$, $L_{DM}{=}64$, $L_r{=}64$, $u{=}[7, 57]$, $L_A{=}4$ |
| $R{=}5.0$: $Q{=}4$, $L{=}32$, $L_{DM}{=}128$, $L_r{=}128$, $u{=}[127, 97]$, $L_A{=}4$ | $R{=}5.5$: $Q{=}4$, $L{=}32$, $L_{DM}{=}128$, $L_r{=}128$, $u{=}[127, 97]$, $L_A{=}8$ |
| $R{=}6.0$: $Q{=}8$, $L{=}32$, $L_{DM}{=}256$, $L_r{=}256$, $u{=}[11, 237]$, $L_A{=}8$ | |

(b) DSTSK-DAST, SE-APSK, $M = T = 2$

| | |
|---|---|
| $R = 2.5$: $Q = 2$, $L = 8$, $L_{DM} = 16$, $u = [1, 9]$, $L_A = 2$ | $R = 3.0$: $Q = 4$, $L = 8$, $L_{DM} = 32$, $u = [1, 25]$, $L_A = 2$ |
| $R = 3.5$: $Q = 4$, $L = 16$, $L_{DM} = 64$, $u = [15, 63]$, $L_A = 2$ | $R = 4.0$: $Q = 4$, $L = 16$, $L_{DM} = 64$, $u = [15, 63]$, $L_A = 4$ |
| $R = 4.5$: $Q = 8$, $L = 16$, $L_{DM} = 128$, $u = [1, 81]$, $L_A = 4$ | $R = 5.0$: $Q = 8$, $L = 32$, $L_{DM} = 256$, $u = [1, 161]$, $L_A = 4$ |
| $R = 5.5$: $Q = 8$, $L = 32$, $L_{DM} = 256$, $u = [1, 161]$, $L_A = 8$ | $R = 6.0$: $Q = 8$, $L = 64$, $L_{DM} = 512$, $u = [319, 511]$, $L_A = 8$ |

(c) DGC-cyclic, SE-APSK, $M = T = 2$

| | | |
|---|---|---|
| $R = 2.5$: $L = 16$, $u = [1, 7]$, $L_A = 2$ | $R = 3.0$: $L = 32$, $u = [1, 7]$, $L_A = 2$ | $R = 3.5$: $L = 64$, $u = [1, 19]$, $L_A = 2$ |
| $R = 4.0$: $L = 64$, $u = [1, 19]$, $L_A = 4$ | $R = 4.5$: $L = 128$, $u = [1, 47]$, $L_A = 4$ | $R = 5.0$: $L = 256$, $u = [1, 75]$, $L_A = 4$ |
| $R = 5.5$: $L = 256$, $u = [1, 75]$, $L_A = 8$ | $R = 6.0$: $L = 512$, $u = [1, 149]$, $L_A = 8$ | |

(d) DSTSK-TAST, $M = T = 4$

| | |
|---|---|
| $R{=}1.5$: $Q{=}2$, $L{=}8$, $L_{DM}{=}16$, $L_r{=}32$, $u{=}[1, 5, 11, 15]$ | $R{=}1.75$: $Q{=}4$, $L{=}8$, $L_{DM}{=}32$, $L_r{=}32$, $u{=}[5, 25, 11, 31]$ |
| $R{=}2.0$: $Q{=}8$, $L{=}8$, $L_{DM}{=}64$, $L_r{=}64$, $u{=}[15, 41, 57, 63]$ | $R{=}2.25$: $Q{=}8$,$L{=}16$,$L_{DM}{=}128$,$L_r{=}128$,$u{=}[31, 89, 113, 127]$ |
| $R{=}2.5$: $Q{=}16$, $L{=}16$, $L_{DM}{=}256$, $L_r{=}256$, $u{=}[1, 41, 55, 135]$ | $R{=}2.75$: $Q{=}32$,$L{=}16$,$L_{DM}{=}512$,$L_r{=}512$,$u{=}[71, 41, 489, 503]$ |
| $R{=}3.0$:$Q{=}64$,$L{=}16$,$L_{DM}{=}1024$,$L_r{=}1024$,$u{=}[633, 603, 559, 797]$ | |

(e) DSTSK-DAST, $M = T = 4$

| | |
|---|---|
| $R{=}1.5$: $Q{=}8$, $L{=}8$, $L_{DM}{=}64$, $u{=}[7, 23, 47, 63]$ | $R{=}1.75$: $Q{=}16$, $L{=}8$, $L_{DM}{=}128$, $u{=}[71, 79, 119, 127]$ |
| $R{=}2.0$: $Q{=}32$, $L{=}8$, $L_{DM}{=}256$, $u{=}[1, 41, 49, 137]$ | $R{=}2.25$: $Q{=}32$, $L{=}16$, $L_{DM}{=}512$, $u{=}[49, 193, 401, 513]$ |
| $R{=}2.5$: $Q{=}64$, $L{=}16$, $L_{DM}{=}1024$, $u{=}[5, 999, 1303, 2587]$ | $R{=}2.75$: $Q{=}64$, $L{=}32$, $L_{DM}{=}2048$, $u{=}[1119, 2047, 2271, 2687]$ |
| $R{=}3.0$: $Q{=}128$, $L{=}32$, $L_{DM}{=}4096$, $u{=}[4045_7 693_1 2045_1 1501]$ | |

(f) DGC-cyclic, $M = T = 4$

| | | |
|---|---|---|
| $R = 2.25$: $L = 512$, $u = [1, 67, 123, 231]$ | $R = 2.5$: $L = 1024$, $u = [1, 187, 221, 351]$ | $R = 2.75$: $L = 2048$, $u = [1, 277, 325, 919]$ |
| $R = 3$: $L = 4096$, $u = [1, 493, 695, 1851]$ | | |

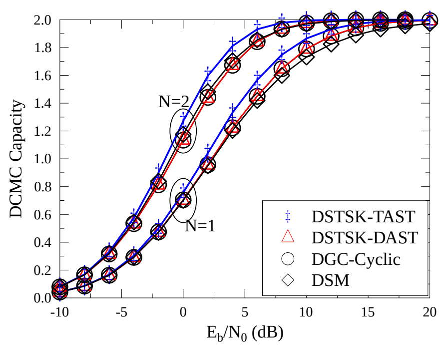


(a) DCMC capacity

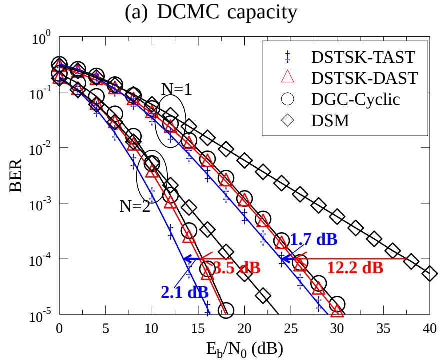


(b) BER performance

Fig. 9: DCMC capacity and BER comparison of DSTM schemes associated with $M = T = 2$ and $R = 2.0$. The DSTSK-DAST's diversity gains over DSM at BER=$10^{-4}$ are marked by red arrows, while the DSTSK-TAST's performance improvements over DGC at BER=$10^{-4}$ are marked by blue arrows.

TABLE XII: Complexity (number of real-valued multiplications) of DSTM schemes.

| | Using PSK | Using APSK |
|---|---|---|
| DSTSK-TAST | $4NT^2 + 4T^2Q + 5TQ$ | $4NT^2 + 4T^2Q + 5TQ + 2N + 3$ |
| DSTSK-DAST | $4NT^2 + 4TQ + 5Q$ | $4NT^2 + 4TQ + 5Q + 2N + 3$ |
| DGC-cyclic | $4NT^2 + 5TL$ | $4NT^2 + 5TL + 2N + 3$ |
| FE-DSM | $4NT^2 + 4T^2 + 5T$ | $4NT^2 + 4T^2 + 5T + 2N + 3$ |
| DSTBC-ISK | $4NT^2 + 2NT + 4T$ | $4NT^2 + 2NT + 4T + 2N + 3$ |
| DSM | $4NT^2 + 5Q2^{\lfloor \log_2 T! \rfloor}$ | $4NT^2 + 5Q2^{\lfloor \log_2 T! \rfloor} + 2N + 3$ |
| DPSK/APSK | $4N + 1$ | $6N + 9$ |

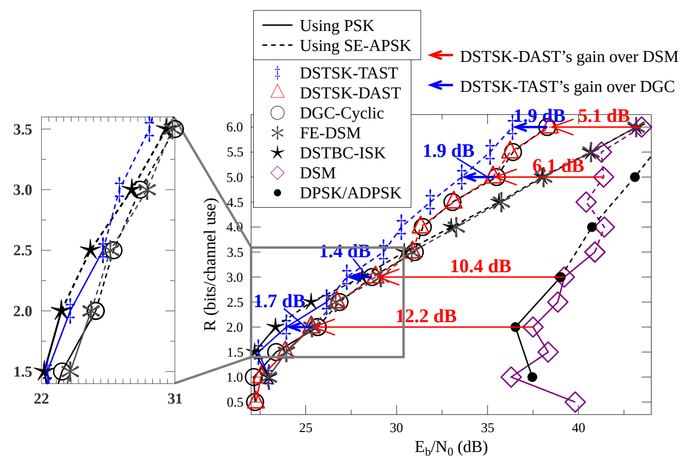


(a) $M = T = 2$

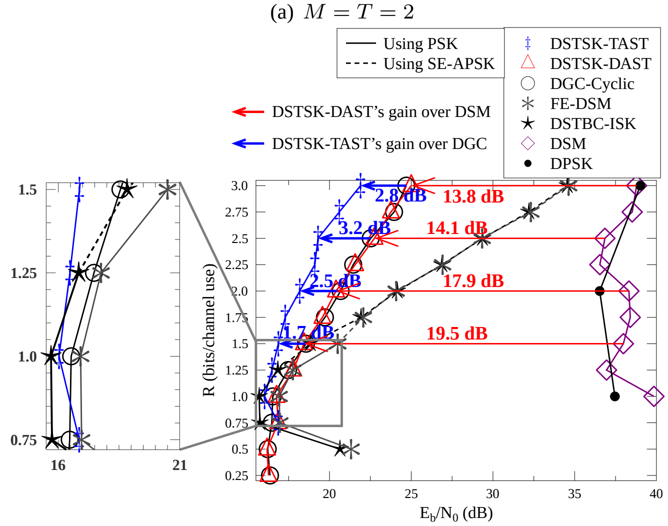


(b) $M = T = 4$

Fig. 10: Comparison of $E_b/N_0$ required for DSTM schemes associated with $M = T = \{2, 4\}$ and $N = 1$ to achieve BER=$10^{-4}$. The DSTSK-DAST's diversity gains over DSM at BER=$10^{-4}$ are marked by red arrows, while the DSTSK-TAST's performance improvements over DGC at BER=$10^{-4}$ are marked by blue arrows.

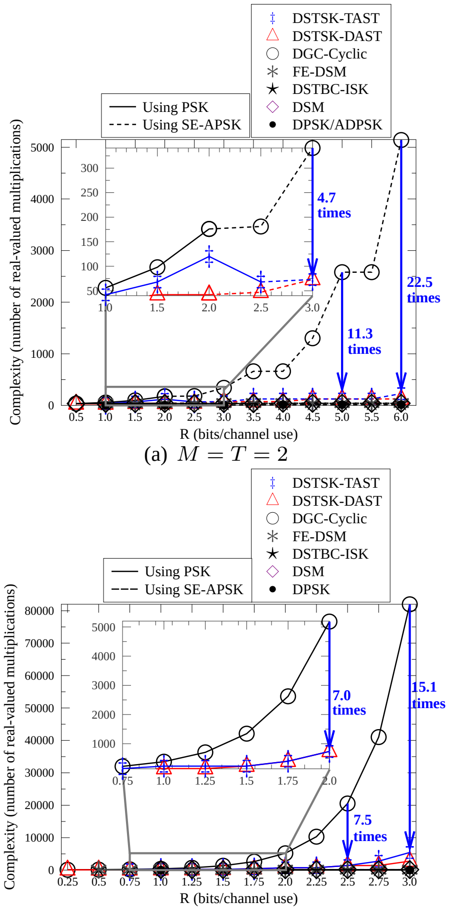


(a) $M = T = 2$

(b) $M = T = 4$

Fig. 11: Complexity comparison for DSTM schemes associated with $M = T = \{2, 4\}$ and $N = 1$, where the DSTSK-TAST's complexity reduction compared to DGC-cyclic are marked by blue arrows.

summarized in Table XII. We also note that the evaluation of the DGC [39], [41]–[43] detection complexity and that of the DSM [31], [32] detection complexity are based on their simplied detectors summaried in [40].

First of all, it is evidenced by Fig. 10 that the DSM does not perform well for a small $N = 1$. Secondly, Fig. 10 demonstrates that DSTBC-ISK outperforms FE-DSM at $1.5 \leq R \leq 4.0$ for $M = T = 2$ and $0.5 \leq R \leq 1.75$ for $M = T = 4$. Moreover, DSTBC-ISK even outperforms DGC-cyclic at the low throughputs of $1.5 \leq R \leq 3.5$ for $M = T = 2$ and $0.75 \leq R \leq 1.25$ for $M = T = 4$, as shown in Fig. 10. However, Fig. 10 also demonstrates that the diversity advantages of both DSTBC-ISK and FE-DSM over DSM diminish, as the throughput increases. By contrast, both the proposed DSTSK-DAST and the classic DGC-cyclic achieve substantial non-diminishing diversity gains over the DSM in Fig. 10, but the DSTSK-DAST's single-stream ML detection complexity is significantly lower than the DGC-cyclic's exponentially increasing complexity portrayed in Fig. 11. Furthermore, the proposed DSTSK-TAST is seen in Fig. 10 to achieve an even better performance than DGC-cyclic, despite its substantially reduced detection complexity seen in Fig. 11.

Specifically, for the case of $M = 2$ and $N = 1$, DSTSK-TAST associated with $R = 3.0$ and $R = 6.0$ achieves **1.4 dB** and **1.9 dB** performance gain over DGC-cyclic in Fig. 10(a) at a **4.7 times** and **22.5 times** lower detection complexity in Fig. 11(a), respectively. Moreover, for the case of $M = 4$ and $N = 1$, DSTSK-TAST associated with $R = 2.5$ and $R = 3.0$ achieves even more significant gains of **3.2 dB** and **2.8 dB** over DGC-cyclic in Fig. 10(b) at a **7.5 times** and **15.1 times** lower complexity in Fig. 11(b), respectively.

We note that the full-transmit-diversity arrangements are particularly beneficial for the popular Unmanned Aerial Vehicles (UAVs) applications, which are envisioned to be an important part of the IoT. More explicitly, grave airframe-induced shadowing [56] is encountered, when the critical air-ground link becomes blocked by the chassis/fuselage of the UAV. It is reported in [56] that using multiple RAs at the Ground Station (GS) is unable to mitigate this problem, but the transmit diversity design [57] using multiple TAs is capable of significantly improving the connectivity. Therefore, we suggest that the proposed finite-cardinality single-RF DSTSK-DAST and DSTSK-TAST may become suitable candidates for the UAV applications as a benefit of their low complexity and maximized transmit diversity gain, as discussed in [56]–[58] and the references within.

### B. Diversity-Throughput Tradeoff

In this section, the ME-APSK design and the DR design are applied to the diversity-oriented DSTM schemes of DSTSK-TAST and DSTBC-ISK for a variety of different MIMO system setups. More explicitly, DSTSK-TAST and DSTBC-ISK are compared to DSM for $M = T = \{2, 4\}$ and $N = \{1, 2, 4, 8, 16\}$ both at low and high throughputs of $R = \{2.0, 5.0\}$ in Figs. 12(a)-(d). First of all, although DSTBC-ISK achieves a better performance for $M = T = 2$ and $N = 1$ at a low $R = 2.0$ in Fig. 12(a), its diversity gain diminishes, as the number of RAs $N$ and/or the throughput $R$ increase, as seen in Figs. 12(a)-(d). By contrast, although the DSTSK-TAST's diversity gain over DSM also decreases upon increasing $N$, Figs. 12(a)-(d) manifestly demonstrate that the proposed DSTSK-TAST is capable of achieving a persistent performance advantage over DSM for the cases of $M = T = \{2, 4\}$ using both small and large number of RAs $N = \{1, 2, 4, 8, 16\}$ at both low and high throughputs $R = \{2.0, 5.0\}$. Once again, DSTSK-TAST shares the same low transceiver complexity as the DSM, including the finite-cardinality single-RF transmitter and the single-stream ML receiver architectures.

In conclusion, based on our extensive simulations, we suggest that the DSTBC-ISK using the simple STBC signal structure is beneficial for the cases of using a small number of RAs $N = \{1, 2\}$ at low throughputs, such as $R \leq 3.0$ for $M = 2$ and $R \leq 1.5$ for $M = 4$. Furthermore, with the help of the ME-APSK design and the DR design, the DSTSK-TAST is capable of achieving a persistent performance advantage for a variety of different MIMO system setups, such as $M = T = \{2, 4\}$ and $N \in [1, 16]$ at $R \leq 6.0$. Nonetheless, we also note that the construction of the DSTSK-TAST signal matrix becomes extremely challenging at very high throughputs of $R > 6.0$, where the DSM is preferred especially for using $N > 2$.

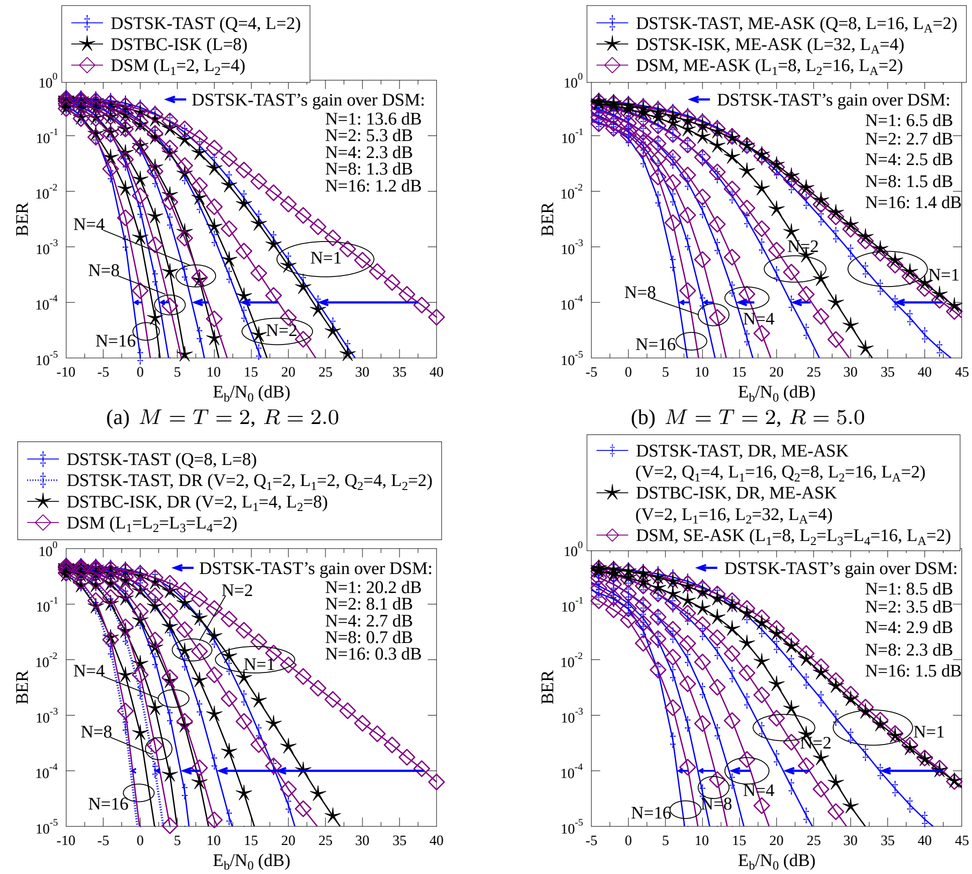


(a) $M = T = 2,\ R = 2.0$ (b) $M = T = 2,\ R = 5.0$

(c) $M = T = 4,\ R = 2.0$ (d) $M = T = 4,\ R = 5.0$

Fig. 12: Performance comparison between the DSTSK-TAST, DSTBC-ISK and DSM arrangements for $M = T = \{2, 4\}$ and $N = \{1, 2, 4, 8, 16\}$ at $R = \{2.0, 5.0\}$. The diversity gains of DSTSK-TAST over DSM at BER=$10^{-4}$ are marked by blue arrows and also listed in figures.

## VII. Conclusions

In summary, our proposed finite-cardinality single-RF DSTM schemes of DSTSK-DAST and DSTSK-TAST mitigate the problem of the diminishing diversity gain of FE-DSM and DSTBC-ISK over DSM, without compromising its appealingly low transceiver complexity. In order to improve the throughput of the diversity-oriented DSTM schemes, we also conceived the ME-APSK and the DR designs, which assists the proposed DSTSK-TAST in achieving a persistent performance advantage over DSM for a variety of MIMO system setups.

## References

[1] S. M. Alamouti, "A simple transmit diversity technique for wireless communications," *IEEE J. Sel. Areas Commun.*, vol. 16, pp. 1451–1458, Oct. 1998.

[2] V. Tarokh, H. Jafarkhani, and A. R. Calderbank, "Space-time block codes from orthogonal designs," *IEEE Trans. Inf. Theory*, vol. 45, pp. 1456–1467, July 1999.

[3] G. Ganesan and P. Stoica, "Space-time block codes: a maximum SNR approach," *IEEE Trans. Inf. Theory*, vol. 47, pp. 1650–1656, May 2001.

[4] V. Tarokh and H. Jafarkhani, "A differential detection scheme for transmit diversity," *IEEE J. Sel. Areas Commun.*, vol. 18, pp. 1169–1174, July 2000.

[5] H. Jafarkhani and V. Tarokh, "Multiple transmit antenna differential detection from generalized orthogonal designs," *IEEE Trans. Inf. Theory*, vol. 47, pp. 2626–2631, Sept. 2001.

[6] G. Ganesan and P. Stoica, "Differential modulation using space-time block codes," *IEEE Signal Process. Lett.*, vol. 9, pp. 57–60, Feb 2002.

[7] M. O. Damen, K. Abed-Meraim, and J. C. Belfiore, "Diagonal algebraic space-time block codes," *IEEE Trans. Inf. Theory*, pp. 628–636, 2002.

[8] B. Hassibi and B. M. Hochwald, "High-rate codes that are linear in space and time," *IEEE Trans. Inf. Theory*, pp. 1804–1824, 2002.

[9] R. W. Heath and A. J. Paulraj, "Linear dispersion codes for MIMO systems based on frame theory," *IEEE Trans. Signal Process.*, vol. 50, pp. 2429–2441, Oct 2002.

[10] H. E. Gamal and M. O. Damen, "Universal space-time coding," *IEEE Trans. Inf. Theory*, vol. 49, pp. 1097–1119, May 2003.

[11] B. A. Sethuraman, B. S. Rajan, and V. Shashidhar, "Full-diversity, high-rate space-time block codes from division algebras," *IEEE Trans. Inf. Theory*, vol. 49, pp. 2596–2616, Oct 2003.

[12] B. Hassibi and B. M. Hochwald, "Cayley differential unitary space-time codes," *IEEE Trans. Inf. Theory*, vol. 48, pp. 1485–1503, Jun 2002.

[13] F. Oggier, "Cyclic algebras for noncoherent differential space-time coding," *IEEE Trans. Inf. Theory*, vol. 53, pp. 3053–3065, Sept 2007.

[14] S. Sugiura, S. Chen, and L. Hanzo, "Coherent and differential space-time shift keying: A dispersion matrix approach," *IEEE Trans. Commun.*, vol. 58, pp. 3219–3230, November 2010.

[15] S. Sugiura, C. Xu, S. X. Ng, and L. Hanzo, "Reduced-complexity coherent versus non-coherent QAM-aided space-time shift keying," *IEEE Trans. Commun.*, vol. 59, pp. 3090–3101, November 2011.

[16] C. Xu, S. Sugiura, S. X. Ng, and L. Hanzo, "Reduced-complexity non-coherently detected differential space-time shift keying," *IEEE Signal Process. Lett.*, vol. 18, pp. 153–156, March 2011.

[17] C. Xu, S. Sugiura, S. X. Ng, and L. Hanzo, "Spatial modulation and space-time shift keying: Optimal performance at a reduced detection complexity," *IEEE Trans. Commun.*, vol. 61, pp. 206–216, January 2013.

[18] R. Rajashekar, K. V. S. Hari, and L. Hanzo, "Reduced-complexity ML detection and capacity-optimized training for spatial modulation systems," *IEEE Trans. Commun.*, vol. 62, pp. 112–125, January 2014.

[19] J. G. Proakis, *Digital Communications*. New York: McGraw-Hill, 1995.

[20] A. Goldsmith, *Wireless communications*. Cambridge Uni. Press, 2005.

[21] W. Webb, L. Hanzo, and R. Steele, "Bandwidth efficient QAM schemes for Rayleigh fading channels," *IEE Proc. I, Commun., Speech and Vision*, vol. 138, no. 3, pp. 169–175, June 1991.

[22] L. Hanzo, O. Alamri, M. El-Hajjar, and N. Wu, *Near-Capacity Multi-Functional MIMO Systems: Sphere-Packing, Iterative Detection and Cooperation*. John Wiley & Sons, May 2009.

[23] L. Lampe and R. Schober, "Low-complexity iterative demodulation for noncoherent coded transmission over Ricean-fading channels," *IEEE Trans. Veh. Technol.*, vol. 50, no. 6, pp. 1481–1496, Nov. 2001.
[24] C. Xu, S. X. Ng, and L. Hanzo, "Multiple-symbol differential sphere detection and decision-feedback differential detection conceived for differential QAM," *IEEE Trans. Veh. Technol.*, pp. 8345–8360, 2016.
[25] C. Xu, L. Wang, S. X. Ng, and L. Hanzo, "Soft-decision multiple-symbol differential sphere detection and decision-feedback differential detection for differential QAM dispensing with channel estimation in the face of rapidly fading channels," *IEEE Trans. Wireless Commun.*, vol. 15, pp. 4408–4425, June 2016.
[26] A. Kalis, A. G. Kanatas, and C. B. Papadias, "A novel approach to MIMO transmission using a single RF front end," *IEEE J. Sel. Areas Commun.*, vol. 26, pp. 972–980, August 2008.
[27] O. N. Alrabadi, C. B. Papadias, A. Kalis, and R. Prasad, "A universal encoding scheme for MIMO transmission using a single active element for PSK modulation schemes," *IEEE Trans. Wireless Commun.*, vol. 8, pp. 5133–5142, October 2009.
[28] S. Sugiura, "Coherent versus non-coherent reconfigurable antenna aided virtual MIMO systems," *IEEE Signal Process. Lett.*, vol. 21, pp. 390–394, April 2014.
[29] R. Y. Mesleh, H. Haas, S. Sinanovic, C. W. Ahn, and S. Yun, "Spatial modulation," *IEEE Trans. Veh. Technol.*, vol. 57, pp. 2228–2241, 2008.
[30] P. Yang, M. D. Renzo, Y. Xiao, S. Li, and L. Hanzo, "Design guidelines for spatial modulation," *IEEE Communications Surveys Tutorials*, vol. 17, pp. 6–26, Firstquarter 2015.
[31] Y. Bian, M. Wen, X. Cheng, H. V. Poor, and B. Jiao, "A differential scheme for spatial modulation," in *IEEE Global Commun. Conf.*, pp. 3925–3930, Dec 2013.
[32] Y. Bian, X. Cheng, M. Wen, L. Yang, H. V. Poor, and B. Jiao, "Differential spatial modulation," *IEEE Trans. Veh. Technol.*, vol. 64, pp. 3262–3268, July 2015.
[33] P. A. Martin, "Differential spatial modulation for APSK in time-varying fading channels," *IEEE Commun. Lett.*, vol. 19, pp. 1261–1264, 2015.
[34] J. Liu, L. Dan, P. Yang, L. Xiao, F. Yu, and Y. Xiao, "High-rate APSK-aided differential spatial modulation: Design method and performance analysis," *IEEE Commun. Lett.*, vol. PP, no. 99, pp. 1–1, 2016.
[35] X. Cheng, M. Zhang, M. Wen, and L. Yang, "Index modulation for 5G: Striving to do more with less," *IEEE Wireless Commun.*, vol. 25, pp. 126–132, April 2018.
[36] M. Zhang, M. Wen, X. Cheng, and L. Yang, "A dual-hop virtual MIMO architecture based on hybrid differential spatial modulation," *IEEE Trans. Wireless Commun.*, vol. 15, pp. 6356–6370, Sept 2016.
[37] R. Rajashekar, N. Ishikawa, S. Sugiura, K. V. S. Hari, and L. Hanzo, "Full-diversity dispersion matrices from algebraic field extensions for differential spatial modulation," *IEEE Trans. Veh. Technol.*, vol. 66, pp. 385–394, Jan 2017.
[38] R. Rajashekar, C. Xu, N. Ishikawa, S. Sugiura, K. V. S. Hari, and L. Hanzo, "Algebraic differential spatial modulation is capable of approaching the performance of its coherent counterpart," *IEEE Trans. Commun.*, vol. 65, pp. 4260–4273, Oct 2017.
[39] A. Shokrollahi, B. Hassibi, B. M. Hochwald, and W. Sweldens, "Representation theory for high-rate multiple-antenna code design," *IEEE Trans. on Inf. Theory*, vol. 47, pp. 2335–2367, Sep 2001.
[40] C. Xu, R. Rajashekar, N. Ishikawa, S. Sugiura, and L. Hanzo, "Single-RF index shift keying aided differential space-time block coding," *IEEE Trans. Signal Process.*, vol. 66, pp. 773–788, Feb 2018.
[41] B. L. Hughes, "Differential space-time modulation," *IEEE Trans. Inf. Theory*, vol. 46, pp. 2567–2578, Nov 2000.
[42] B. M. Hochwald and W. Sweldens, "Differential unitary space-time modulation," *IEEE Trans. Commun.*, vol. 48, pp. 2041–2052, Dec 2000.
[43] B. L. Hughes, "Optimal space-time constellations from groups," *IEEE Trans. Inf. Theory*, vol. 49, pp. 401–410, Feb 2003.
[44] P. Yang, Y. Xiao, Y. L. Guan, K. V. S. Hari, A. Chockalingam, S. Sugiura, H. Haas, M. D. Renzo, C. Masouros, Z. Liu, L. Xiao, S. Li, and L. Hanzo, "Single-carrier SM-MIMO: A promising design for broadband large-scale antenna systems," *IEEE Commun. Surveys Tutorials*, vol. 18, pp. 1687–1716, thirdquarter 2016.
[45] B. S. Krongold and D. L. Jones, "PAR reduction in OFDM via active constellation extension," *IEEE Trans. Broadcast.*, vol. 49, pp. 258–268, Sept 2003.
[46] Y. J. Kou, W. s. Lu, and A. Antoniou, "A new peak-to-average power-ratio reduction algorithm for OFDM systems via constellation extension," *IEEE Trans. Wireless Commun.*, vol. 6, pp. 1823–1832, May 2007.
[47] Y. Wang, W. Chen, and C. Tellambura, "Genetic algorithm based nearly optimal peak reduction tone set selection for adaptive amplitude clipping PAPR reduction," *IEEE Trans. Broadcast.*, vol. 58, pp. 462–471, Sept 2012.
[48] S. H. Han and J. H. Lee, "An overview of peak-to-average power ratio reduction techniques for multicarrier transmission," *IEEE Wireless Commun.*, vol. 12, pp. 56–65, April 2005.
[49] B. M. Hochwald and T. L. Marzetta, "Unitary space-time modulation for multiple-antenna communications in Rayleigh flat fading," *IEEE Trans. Inf. Theory*, vol. 46, pp. 543–564, Mar 2000.
[50] X. Liang and X. Xia, "Unitary signal constellations for differential space-time modulation with two transmit antennas: parametric codes, optimal designs, and bounds," *IEEE Trans. Inf. Theory*, vol. 48, pp. 2291–2322, Aug 2002.
[51] X. Giraud, E. Boutillon, and J. C. Belfiore, "Algebraic tools to build modulation schemes for fading channels," *IEEE Trans. Inf. Theory*, vol. 43, pp. 938–952, May 1997.
[52] V. M. DaSilva and E. S. Sousa, "Fading-resistant modulation using several transmitter antennas," *IEEE Trans. Commun.*, pp. 1236–1244, 1997.
[53] J. Boutros and E. Viterbo, "Signal space diversity: a power- and bandwidth-efficient diversity technique for the Rayleigh fading channel," *IEEE Trans. Inf. Theory*, vol. 44, pp. 1453–1467, Jul 1998.
[54] J. Wang, X. Wang, and M. Madihian, "Design of minimum error-rate Cayley differential unitary space-time codes," *IEEE J. Sel. Areas Commun.*, vol. 23, pp. 1779–1787, Sept 2005.
[55] S. Sugiura and L. Hanzo, "On the joint optimization of dispersion matrices and constellations for near-capacity irregular precoded space-time shift keying," *IEEE Trans. Wireless Commun.*, vol. 12, pp. 380–387, January 2013.
[56] R. Sun, D. W. Matolak, and W. Rayess, "Air-ground channel characterization for unmanned aircraft systems – part IV: Airframe shadowing," *IEEE Trans. Veh. Technol.*, vol. 66, pp. 7643–7652, Sept 2017.
[57] M. A. Jensen, M. D. Rice, and A. L. Anderson, "Aeronautical telemetry using multiple-antenna transmitters," *IEEE Trans. Aerosp. Electron. Syst.*, vol. 43, pp. 262–272, January 2007.
[58] S. Hayat, E. Yanmaz, and R. Muzaffar, "Survey on unmanned aerial vehicle networks for civil applications: A communications viewpoint," *IEEE Commun. Surveys Tuts.*, vol. 18, pp. 2624–2661, Fourthquarter 2016.

**Chao Xu** (S'09-M'14) received a B.Eng. degree from Beijing University of Posts and Telecommunications, China, and a BSc(Eng) with First Class Honours from Queen Mary, University of London, UK, through a Sino-UK joint degree program in 2008, both in Telecommunications Enginneering with Management. He obtained a MSc degree with distinction in Radio Frequency Communication Systems and a Ph.D. degree in Wireless Communications from the University of Southampton, UK in 2009 and 2015, respectively. He is currently a postdoctoral researcher working at Southampton Wireless Group, University of Southampton, UK. His research interests include index modulation, reduced-complexity MIMO design, noncoherent detection and turbo detection. He was awarded the Best M.Sc. Student in Broadband and Mobile Communication Networks by the IEEE Communications Society (United Kingdom and Republic of Ireland Chapter) in 2009. He also received 2012 Chinese Government Award for Outstanding Self-Financed Student Abroad.

**Peichang Zhang** received the B.Eng. degree (with first-class honor) in electronic engineering from the University of Central Lancashire, Preston, U.K., in 2009 and the M.Sc. and Ph.D degree in wireless communications from the University of Southampton, Southampton, U.K., in 2010 and 2015, respectively. He is now with the College of Information and Engineering, Shenzhen University, China. His research interests include antenna selection, coherent and non-coherent detection, iterative detection, as well as channel estimation.

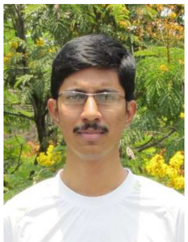

**Rakshith Rajashekar** (M'14-SM'17) received the B.E. degree in electrical communication engineering from Visvesvaraya Technological University, Karnataka, India, in 2007. He received his Ph.D. from the Department of Electrical Communication Engineering, Indian Institute of Science (IISc), India, in 2014. He is presently working as a Research Fellow at the University of Southampton, UK. Before joining the University of Southampton, he worked at Accord Software & Systems, Bengaluru, India, as a Systems Engineer from 2007 to 2009, and as a Senior Scientist at Broadcom Communications, Bengaluru, India from 2014 to 2015. His research interests include antenna selection in MIMO systems, differential communication, millimeter wave communication, communication between drones with a focus on space-time signal processing and coding. He is the recipient of the Special Recognition award from Broadcom Communications, India and the Dean's Award from the University of Southampton, UK, for excellence in research. He has received the Best Reviewer award from IEEE Transactions on Wireless Communications, IEEE Transactions on Communications and IEEE Wireless Communications Letters.

**Naoki Ishikawa** (S'13–M'17) was born in Kanagawa, Japan, in 1991. He received the B.E., M.E., and Ph.D. degrees from the Tokyo University of Agriculture and Technology, Tokyo, Japan, in 2014, 2015, and 2017, respectively. From June 2015 to September 2015, he was an academic visitor with the School of Electronics and Computer Science, University of Southampton, UK. From April 2016 to March 2017, he was a research fellow of the Japan Society for the Promotion of Science. From April 2017, he has been an assistant professor in the Graduate School of Information Sciences, Hiroshima City University, Japan.

He was certified as an Exemplary Reviewer of IEEE TRANSACTIONS ON COMMUNICATIONS 2017. He also received eight domestic awards, including the Yasujiro Niwa Outstanding Paper Award from Tokyo Denki University in 2018, the Telecom System Technology student Award (honorable mention) from Telecommunications Advancement Foundation of Japan in 2014, and the Outstanding Paper Award for Young C&C Researchers from NEC C&C Foundation in 2014.

**Shinya Sugiura** (M'06–SM'12) received the B.S. and M.S. degrees in aeronautics and astronautics from Kyoto University, Kyoto, Japan, in 2002 and 2004, respectively, and the Ph.D. degree in electronics and electrical engineering from the University of Southampton, Southampton, U.K., in 2010.

From 2004 to 2012, he was a Research Scientist with Toyota Central Research and Development Laboratories, Inc., Aichi, Japan. From 2013 to 2018, he was an Associate Professor with the Department of Computer and Information Sciences, Tokyo University of Agriculture and Technology, Tokyo, Japan. Since 2018, he has been an Associate Professor with the Institute of Industrial Science, University of Tokyo, Tokyo, Japan, where he heads the Wireless Communications Research Group. His research has covered a range of areas in wireless communications, networking, signal processing, and antenna technology. He authored or coauthored over 60 IEEE journal papers.

Dr. Sugiura was a recipient of a number of awards, including the Sixth RIEC Award from the Foundation for the Promotion of Electrical Communication in 2016, the Young Scientists' Prize by the Minister of Education, Culture, Sports, Science and Technology of Japan in 2016, the 14th Funai Information Technology Award (First Prize) from the Funai Foundation in 2015, the 28th Telecom System Technology Award from the Telecommunications Advancement Foundation in 2013, the Sixth IEEE Communications Society Asia-Pacific Outstanding Young Researcher Award in 2011, the 13th Ericsson Young Scientist Award in 2011, and the 2008 IEEE Antennas and Propagation Society Japan Chapter Young Engineer Award. He was also certified as an Exemplary Reviewer of IEEE COMMUNICATIONS LETTERS in 2013 and 2014, and that of IEEE TRANSACTIONS ON COMMUNICATIONS in 2018.

**Li Wang** received his Ph.D. degree from the University of Southampton, Southampton, U.K., in 2010. From 2010 to 2012, he conducted research as a Senior Research Fellow with the School of Electronics and Computer Science, University of Southampton. During his academic period, he was involved in a number of projects, such as those from UK's EPSRC, Mobile VCE and Indian-UK Advanced Technology Centre (IU-ATC). In March 2012, he joined the R&D Center of Huawei Technologies in Stockholm, Sweden, and is currently working as a Principle Research Engineer in Wireless Network Algorithm Lab. He has authored 40+ research papers in IEEE/IET journals and conferences, and also coauthored one John Wiley/IEEE Press book. He has wide research interests in both radio transmission technology (RTT) and radio resource management (RRM) areas for future wireless communication technologies and networks. He has also been conducting pioneering cross-discipline researches to build next-generation communication systems with artificial intelligence (AI) since 2013. In recognition of his contributions in this field, he was the recipient of Huawei Individual Contribution Award in 2015 and Future Star Award in 2017. He is Cambridge University Issac Newton Institute Member and IEEE Senior Member.

**Lajos Hanzo** (M'91-SM'92-F'04) (http://www-mobile.ecs.soton.ac.uk) FREng, FIEEE, FIET, Fellow of EURASIP, DSc received his degree in electronics in 1976 and his doctorate in 1983. In 2009 he was awarded an honorary doctorate by the Technical University of Budapest, while in 2015 by the University of Edinburgh. During his 40-year career in telecommunications he has held various research and academic posts in Hungary, Germany and the UK. Since 1986 he has been with the School of Electronics and Computer Science, University of Southampton, UK, where he holds the chair in telecommunications. He has successfully supervised about 100 PhD students, co-authored 20 John Wiley/IEEE Press books on mobile radio communications totalling in excess of 10 000 pages, published 1500+ research entries at IEEE Xplore, acted both as TPC and General Chair of IEEE conferences, presented keynote lectures and has been awarded a number of distinctions. Currently he is directing a 60-strong academic research team, working on a range of research projects in the field of wireless multimedia communications sponsored by industry, the Engineering and Physical Sciences Research Council (EPSRC) UK, the European Research Council's Advanced Fellow Grant and the Royal Society's Wolfson Research Merit Award. He is an enthusiastic supporter of industrial and academic liaison and he offers a range of industrial courses. He is also a Governor of the IEEE VTS. During 2008 - 2012 he was the Editor-in-Chief of the IEEE Press and a Chaired Professor also at Tsinghua University, Beijing. His research is funded by the European Research Council's Senior Research Fellow Grant. For further information on research in progress and associated publications please refer to http://www-mobile.ecs.soton.ac.uk Lajos has 24 000 citations.